AD-A153 582 ARTIC MIXED LAYER DYNAMICS(U) WASHINGTON UNIV SEATTLE 1/1
POLAR SCIENCE CENTER J MORISON FEB 85 N00014-83-K-0115

UNCLASSIFIED F/G 8/10 NL

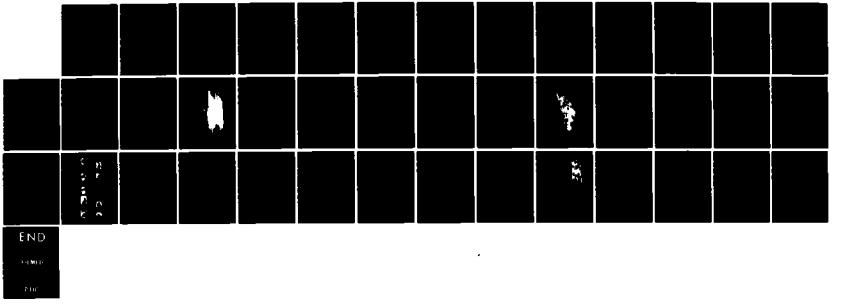

END

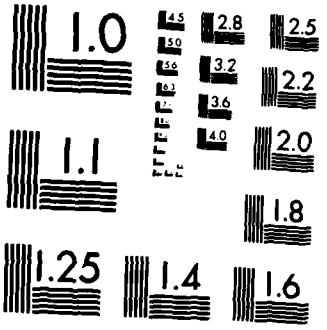

AD-A153 582

F I N A L R E P O R T

ONR Contract N00014-83-K-0115

Arctic Mixed Layer Dynamics

PI: James Morison
University of Washington
Polar Science Center
4057 Roosevelt Way NE
Seattle, WA 98105

February, 1985

FINAL REPORT -- ARCTIC MIXED LAYER DYNAMICS

The ONR contract N00014-83-K-0115 Arctic Mixed Layer Dynamics has covered a wide range of topics related to the dynamics of the upper Arctic Ocean. One of the first projects involved analysis of historical hydrographic data from T-3. This work is described in Appendix A, and it shows the Arctic mixed layer to behave seasonally much like a temperate ocean mixed layer but with salt, rather than temperature, being the active determinant of density.

Participation in the NORSEX experiment was funded under this contract and the results are described in Appendix B. The work produced a wealth of knowledge regarding upper ocean dynamics in the Greenland Sea marginal ice zone. Much of this information formed the basis for the design of the subsequent MIZEX experiments.

In 1981 participation in the Fram III experiment was funded under this contract. The experiment is described in Appendix C and a data report of Arctic Profiling System results is given in Morison and Anderson (1985).

In addition to using the APS at Fram III, a SALARGOS temperature conductivity chain buoy was tested at the site. Buoy development has been carried on in order to develop the means for gathering more long term records of Arctic mixed layer characteristics and gathering internal wave data. The progress in this work is described in Appendix D.

The study of internal waves in the Arctic was stimulated by the realization reached in 1981 and described in Morison (1985), that internal wave energies in the Arctic are lower than in temperate oceans. Additional evidence to this effect was gathered at Fram III and is described in Levine et al., 1985. This work has stimulated the planning of the AIWEX experiment and the discussion of internal wave energy dissipation in Morison et al. (1985).

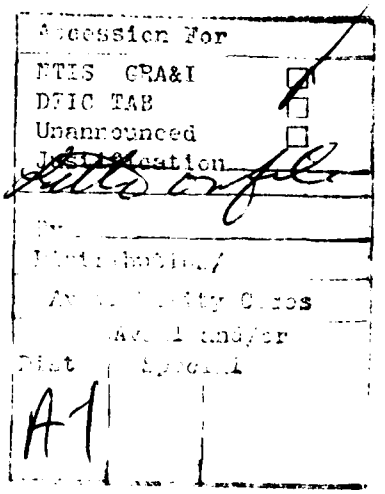

REFERENCES

Levine, M.D., C.A. Paulson, and J.H. Morison. Internal waves in the Arctic Ocean: Observations and comparison with lower latitude climatology. Journ. Phys. Ocean., in press, 1985.

Morison, J.H. Internal Waves in the Arctic: A review. Geophysics of Sea Ice, N. Untersteiner, editor (in press), 1985.

Morison, J.H. and R. Anderson. Profiles of Temperature, Salinity, and Velocity Made with the Arctic Profiling System During Fram III. APL Technical Memo 1-85, 1985.

Morison, J.H., C.E. Long, and M.D. Levine. The dissipation of internal wave energy under Arctic Ice. J. Geophys. Res., in press, 1985.

Appendix A

GEOPHYSICAL RESEARCH LETTERS, VOL. 8, NO. 7, PAGES 753-756, JULY 1981

SEASONAL VARIATIONS IN THE UPPER ARCTIC OCEAN AS OBSERVED AT T-3

James Morison

Polar Science Center University of Washington Seattle, Washington 98195

J. Dungan Smith

Geophysics Program University of Washington Seattle, Washington 98195

Abstract. Hydrographic data from T-3 are analyzed to illustrate the behavior of the Arctic mixed layer. The mixed layer depth fluctuates 11 m annually and mixed layer salinity fluctuates 0.32 ‰. The fluctuations in total salt content are consistent with theoretical work by Maykut and are in phase with mixed layer depth, indicating changes in the mixed layer are controlled by salt flux. Deepening of the mixed layer brings 0.3 kcal cm^{-2} yr^{-1} of heat to the surface from the ocean below.

From 1970 to 1973, a group headed by Dr. T. S. English made hydrocasts using Nansen bottles from the ice island T-3 [Smith and English, 1973]. This paper deals with the seasonal behavior of the upper ocean as illustrated by the resulting data set. The character of the mixed layer is described, results from a model of ice growth and melt are compared with the observations, and the oceanic heat flux is estimated.

Figure 1 shows the positions of T-3 over the period under discussion. The ice island was in the northeast corner of the Canadian Basin and drifted east-southeast toward the northern tip of Ellesmere Island.

Figure 2 shows temperature and σ_t profiles from a typical hydrocast and illustrates the basic features of the density structure of the upper ocean in the region of measurement. The bottle spacing in the upper 70 m was usually 5 m. Because temperatures are uniformly low, σ_t is largely controlled by salinity. The σ_t plot shows the mixed layer to be slightly stratified and 44 m deep. The temperature profile indicates temperatures are close to the freezing point in the mixed layer. It also shows a temperature maximum just below the mixed layer due to the presence of Bering Strait Water. This temperature maximum is an ubiquitous and important feature in the Canadian Basin. Below it the temperature decreases then rises again to a second maximum associated with the Atlantic Water. As suggested by Coachman and Barnes [1961], the presence of the upper maximum indicates heat from the Atlantic Water does not reach the surface. Instead, the oceanic heat flux to the surface comes from the Bering Strait Water.

The seasonal changes in the mixed layer are illustrated by plots of mixed layer depth and salinity. Mixed layer depths were determined for each hydrocast by finding the minimum depth at which a large increase in density occurred. Figure 3 shows the fluctuation of mixed layer depth about a quadratic fit to the full four years of data. The average depth is 46 m and the quadratic fit has been subtracted in order to eliminate the trend and curvature due to the drift of the ice island. The circles indicate actual data and the solid line represents a least squares fit of the annual and semi-annual harmonics. The mixed layer depth increases during fall, winter, and spring, reaching a maximum value 5 m greater than the average by the first of June. By the first week of October the depth decreases to a minimum value 6 m less than the average. The keel depth of T-3 at the time of data collection was about 30 m; therefore it usually did not penetrate the pycnocline. Still T-3 may have induced some local mixing. Estimates of this mixing suggest that its effects on the measured annual and semi-annual cycle of mixed layer depth should be quite small compared to the cumulative effect of mixing by the pack as a whole. Any errors due to internal wave generation by T-3 are assumed to produce a negligible effect on estimates of the seasonal cycle.

Figure 4 shows the vertically averaged salinity in the mixed layer treated in the same way as mixed layer depth. The average mixed layer salinity is 31.45 ‰. It increases to 0.17 ‰ above average by the end of May and decreases to 0.15 ‰ below average by the first part of October. During the summer, a layer of very fresh water typically forms right at the surface, especially at depths less than the mean draft of the ice pack. This layer was not resolved by the sampling method used here and unless the fresh water in this layer was mixed down into the rest of the surface layer it was not accounted for in the annual cycle. In the early fall any unmixed fresh water freezes quickly and is better considered part of the ice cover than the mixed layer. Due to its depth and composition, continuous melting of T-3 during the study period is likely. However, calculations indicate that the amount of fresh water produced would have a negligible effect on the salinity profiles.

An important factor in controlling the behavior of the mixed layer is surface buoyancy flux. In the Arctic this is proportional to salt flux. During freeze up, salt is rejected from the newly formed ice (causing a negative buoyancy flux downward) and during the summer melt, fresh water is added at the surface. Figure 5 shows the fluctuation, about a four year quadratic, of total salt content in the upper 100 m. If it is assumed that horizontal advection produces a negligible annual fluctuation, the oscillations represent the time-integral of salt flux due to freezing and melting at the surface. The solid line is a least squares fit of an annual and semi-annual cycle. The salt content rises to 1.0 gm/cm^2 above average by the end of May and drops to 0.6 gm/cm^2 below average at the end of September. The dashed line is the oscillation in accumulated salt flux as estimated from the results of the model for ice growth and melt by Maykut [1977]. In making the estimate, Maykut's predicted salt flux due to ice growth was used and it was assumed that ice melt produced fresh water which diluted the mixed layer. The predicted cycle agrees well with the observations, both in amplitude and phase. The salt content increase during fall, winter, and spring corresponds to a predicted increase in the average ice thickness of 0.6 m. The rapid drop in summer is of course due to ice melt. Using Maykut's model, the net annual salt production is estimated to be 1.8 gm/cm^2 and the model predicts 0.7 m of ice are exported from the region yearly. The oscillations in ice thickness and

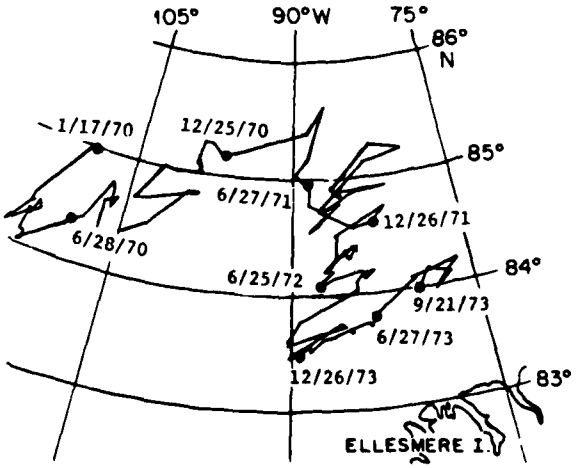

Figure 1. Drift track of T-3, 1970-1973.

Paper number 1L0793.
0094-8276/81/001L-0793$01.00

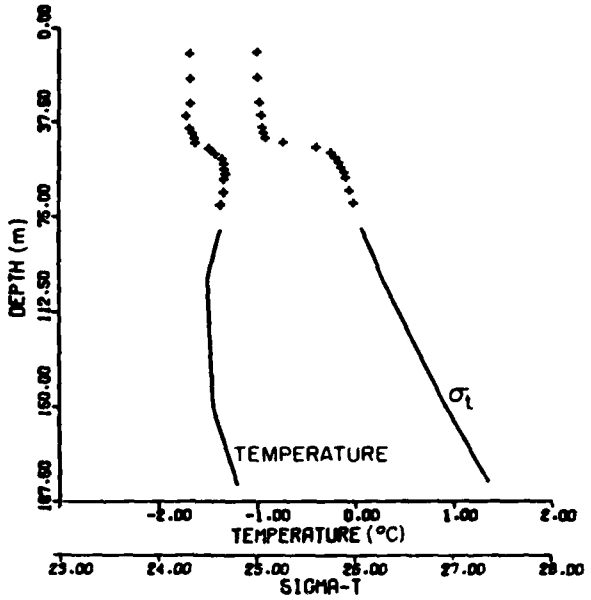

Figure 2. Typical temperature and σ_t profiles from T-3. Note the temperature maximum below the mixed layer. The profile was made 4/26/70.

salt content are nearly the same as these net values. Thus, roughly half of the fresh water removed during freeze up is put back into the ocean during the summer.

The observed behavior of the mixed layer depth resembles the seasonal behavior found in temperate oceans. Also, the change in salinity corresponds to the change in surface temperature at low latitudes. That is, the mixed layer becomes shallow and least dense in summer and becomes deep and most dense in winter. Models such as those of Kraus and Turner [1967], Gill and Turner [1976], Niiler and Kraus [1977] and Garwood [1977] indicate the behavior of the mixed layer is controlled by surface stress and buoyancy flux. The examples given by Kraus and Turner [1967], Gill and Turner [1976] and Garwood [1977] all deal with the idealized situation in which surface stress is assumed to be constant and annual fluctuations in buoyancy flux drive changes in the mixed layer. Such a situation appears to be a reasonable approximation to that found at T-3 because the seasonal fluctuations in wind stress at T-3 are small (only 20% of the four year mean), account for very little of the variance about the mean stress, and do not correlate with changes in mixed layer parameters. On the other hand, variations in total salt content (i.e. buoyancy) show a strong correlation with mixed layer depth and salinity. Comparison of Figure 5 and Figure 3 shows that the curve fits to total salt content and mixed layer depth are almost exactly in phase. The mixed layer salinity is also in phase with the total salt content.

The phase relations displayed by the data during the winter agree qualitatively with those displayed by the models. For example, Figure 8 of Garwood [1977] shows the maximum mixed layer depth occurs at the minimum in heat content. Agreement is not quite as good for the summer season. The models indicate that the minimum mixed layer depth occurs at the maximum in buoyancy flux (downward) and the temperature lags by two to six weeks. The minima in the curve fits for the T-3 mixed layer depth and salinity lag the maximum buoyancy flux by two to three months. Scatter in the data due to interannual variations may account for part of the lag (ex. data points for days 500-730 indicate mixed layer depth lags buoyancy flux by as little as three weeks). However, even allowing for these variations the lag still warrants a physical explanation.

One explanation might be that the mixed layer at T-3 was operating in a strong buoyancy flux regime. Garwood [1977] predicts that with relatively weak variations in buoyancy flux, mixed layer depth and buoyancy flux are nearly in phase during the summer. With a strong buoyancy flux variation, the minimum mixed layer depth lags the maximum buoyancy flux because positive stratification reduces the amount of mechanical energy going into mixing. His Figure 9 shows that with large buoyancy flux (rough estimates of B* at T-3 range from 3 to 7) a slight lag in the minimum depth is produced and deepening is very slow until after the buoyancy flux becomes negative. For such a regime, with the addition of natural short term variations, the minimum measured mixed layer depth might easily be expected to lag the maximum buoyancy flux by two to three months.

The idea that the mixed layer at T-3 was operating in a strong buoyancy flux regime is also supported by the fact that total salt is not only

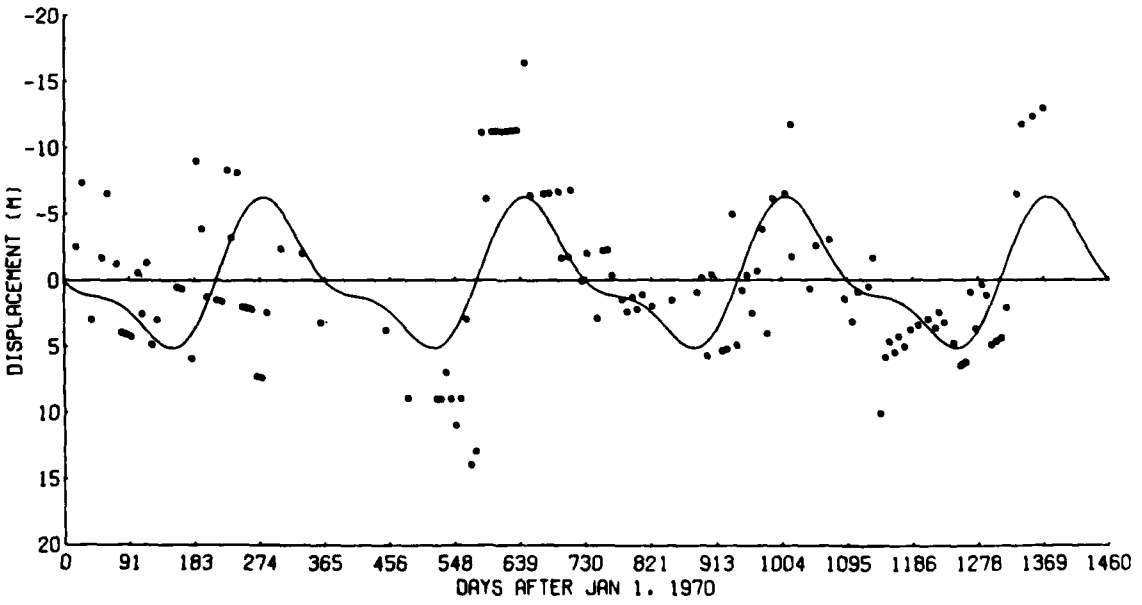

Figure 3. Variation of mixed layer depth about a quadratic fit to four years of data at T-3. The quadratic is $D = 48.0 - (.2598 \times 10^{-1})T + (.2428 \times 10^{-4})T^2$, T = days after 1/1/70. The average depth is 46.0 m. The solid line is a least squares fit of annual and semi-annual cycles.

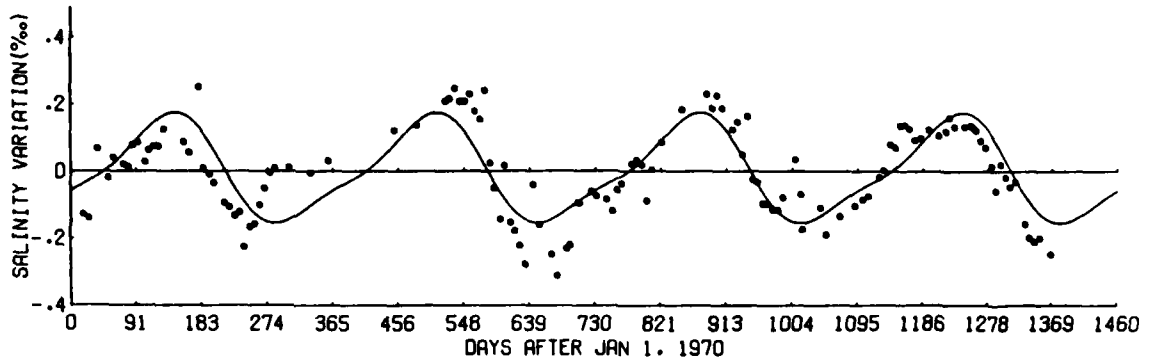

Figure 4. Variation of mixed layer salinity about a quadratic fit to four years of data at T-3. The quadratic is $S = 31.02 - (.3484 \times 10^{-4})T + (.6409 \times 10^{-6})T^2$, T = days after 1/1/70. The average salinity is 31.45‰. The solid line is a least squares fit of annual and semi-annual cycles.

in phase with mixed layer salinity, but can account for nearly all of the mixed layer salinity change. Assuming all the salt is deposited in the average mixed layer depth yields a salinity change of the same magnitude as that observed. (See the axis on the right in Figure 5 and compare to Figure 4.) This aspect of the situation is similar to the first simple example of Gill and Turner [1976] in which wind mixing is ignored completely and mixed layer depth is held constant.

As the mixed layer deepens in the Canadian Basin, heat is entrained from the Bering Strait Water. It is worthwhile to estimate the amount of heat entrained and compare it with estimates made of oceanic heat flux made in other ways. Because the mixed layer is nearly at the freezing point, the heat brought in through mixed layer deepening is simply the product of the mass of water entrained, the temperature elevation above the freezing point of the water below the pycnocline and the heat capacity. This is the oceanic heat available for melting ice. Heat cannot move downward because water at the base of the mixed layer is colder than the water below the pycnocline. By neglecting annual changes in mixed layer depth due to advection and assuming the water entrained is from the Bering Strait Water temperature maximum (water between the base of the mixed layer and the temperature maximum is assumed to be in the process of being mixed), a maximum annual oceanic heat flux can be estimated. The average elevation of the temperature maximum above the freezing point is 0.29°C and the average total winter deepening of the mixed layer is 11.3 m. This yields a heat flux of 0.3 kcal cm^{-2} $year^{-1}$. This value is an order of magnitude less than the 2 kcal cm^{-2} $year^{-1}$ originally suggested by Panov and Sphaiker [1964] and used by Maykut and Untersteiner [1971]. However, Maykut (personal communication) has redone the calculations of Maykut and Untersteiner [1971] and has included the effect of radiation absorbed in open water and through thin ice during summer. These new calculations show that with this radiative contribution and a 2 kcal cm^{-2} $year^{-1}$ oceanic heat flux, the ice cover would melt completely, leading Maykut to conclude that the oceanic heat flux must be much smaller than originally suggested. It should also be added that Panov and Sphaiker's suggested value was based on heat loss from the Atlantic Water which, as pointed out, does in fact not reach the surface in the Canadian Basin.

Finally, it is useful to compare the heat flux estimate above with estimates of horizontal advection of heat in the Bering Strait Water. Aagaard and Griesman [1975] have estimated the transport, average temperature and salinity of the Bering Strait inflow. Using their fig-

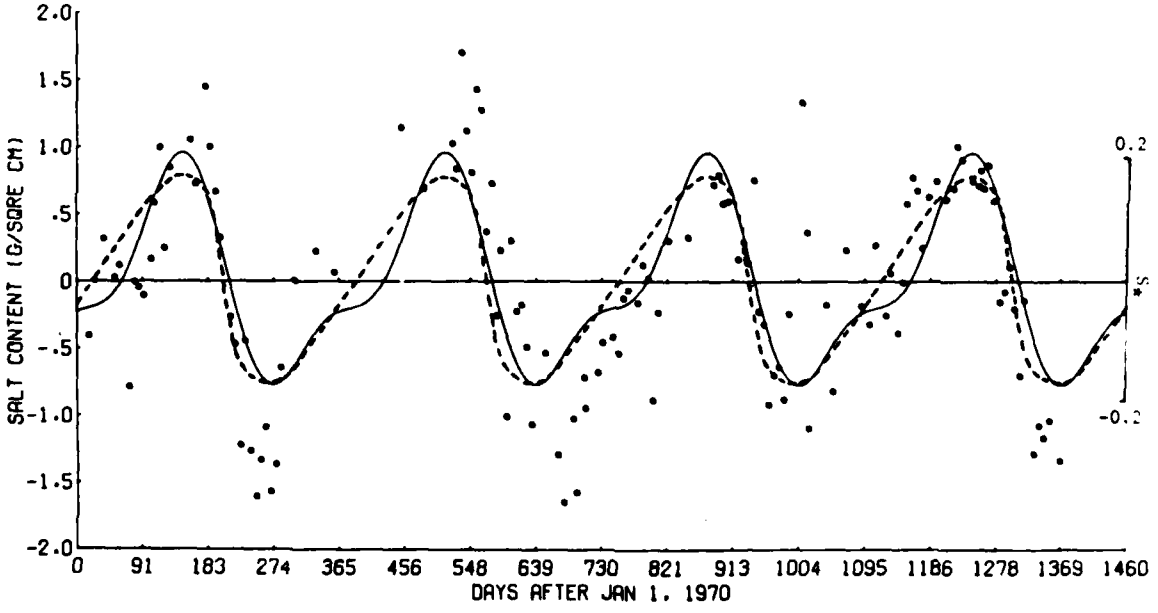

Figure 5. Variation of the salt content in the upper 100 m about a quadratic fit to four years of data at T-3. The quadratic is salt = 324.44 + $(.2182 \times 10^{-2})T + (.2525 \times 10^{-5})T^2$, T = days after 1/1/70. The solid line is a least squares fit of annual and semi-annual cycles. The dashed line is a prediction based on data from Maykut (1977). $S_* = \text{Salt Content} \cdot \text{MLD}^{-1} \cdot \rho^{-1} \cdot 10^3$

ures and computing the heat content relative to the freezing point yields a heat flux. Assuming this must all be lost upward in the Amerasian Basin requires a maximum average oceanic heat flux of 3.0 kcal cm^{-2} $year^{-1}$. However, as Treshnikov [1977] suggests, a large percentage of this heat is probably lost in the seasonal ice zone in the Chukchi Sea. To estimate the heat loss in the northeast corner of the Basin, Bering Strait Water core temperatures and velocities from Coachman and Barnes [1961] can be used. For the region northwest of Ellesmere Island the Bering Strait Water loses 0.12°C while moving southwestward 600 km at a speed of about 1 cm/sec. Assuming the layer is 50 m thick, this corresponds to a heat loss of 0.3 kcal cm^{-2} $year^{-1}$. This value and that obtained from the mixed layer data agree and it suggests that, though 3 kcal cm^{-2} $year^{-1}$ may be a good value on the average, large regions of the Canadian Basin must receive much lower values of oceanic heat flux.

In summary, the T-3 data indicates the mixed layer behavior in the Arctic is controlled by buoyancy flux and the measured fluctuations in salt content agree well with the model of Maykut [1977]. In the region of interest, 0.3 kcal cm^{-2} $year^{-1}$ of heat are entrained into the surface layer from the Bering Strait Water.

Acknowledgments. The authors thank Dr. T. S. English for use of the T-3 data and Sue Geier for her programing efforts. This work was supported by Office of Naval Research Contracts N00014-75-C-0186 and N00014-79-C-0024.

References

Aagaard, K. and P. Greisman, Toward new mass and heat budgets for the Arctic Ocean, J. Geophys. Res., 80(27), 3821-3827, 1975.

Coachman, L. K. and C. A. Barnes, The contribution of Bering Sea water to the Arctic Ocean, Arctic, 14(3), 147-161, 1961.

Garwood, R. A., An oceanic mixed layer model capable of simulating cyclic states, J. of Phys. Oceanogr., 7(3), 455-465, 1977.

Gill, A. E. and J. S. Turner, A comparison of seasonal thermocline models with observations, Deep Sea Research, 23, 391-401, 1976.

Kraus, E. B. and J. S. Turner, A one-dimensional model of the seasonal thermocline: II. The general theory and its consequences, Tellus, 19, 98-106, 1967.

Maykut, G. A., Estimates of the Regional Heat and Mass Balance of the Ice Cover, A Symposium on Sea Ice Processes and Models, 65-74, (Proceedings of symposium held at the University of Washington, Sept. 6-9, 1977.)

Maykut, G. A. and N. Untersteiner, Some results from a time dependent, thermodynamic model of sea ice, J. Geophys. Res., 76(6), 1550-1575, 1971.

Niiler, P. O. and E. B. Kraus, One-dimensional models of the upper ocean, Modeling and Prediction of the Upper Layers of Ocean, E. B. Kraus, Editor, Pergammon Press, New York, 325 pp., 1977.

Panov, V. V. and A. O. Shpaikher, Influence of Atlantic waters upon some features of the hydrology of the Arctic Basin and adjacent seas, Deep Sea Research, 11(2), 275-285, 1964.

Smith, J. D. and T. S. English, Seasonal variations of density and depth of the mixed layer in the Arctic Ocean, (Abstract of oral presentation of the 20th Pacific Northwest Regional Meeting of the American Geophysical Union, Missoula, Montana, October 19, 1973.) EOS, 55(2), 76, 1973.

Treshnikov, A. F., Water masses of the Arctic Basin, Polar Oceans, M. J. Dunbar, Editor, AINA, Calgary, Alberta, 1977.

(Received February 5, 1981;
accepted May 4, 1981.)

Appendix B

JOURNAL OF GEOPHYSICAL RESEARCH, VOL. 88, NO. C5, PAGES 2755–2769, MARCH 30, 1983

Oceanographic Conditions in the Marginal Ice Zone North of Svalbard in Early Fall 1979 With an Emphasis on Mesoscale Processes

O. M. JOHANNESSEN AND J. A. JOHANNESSEN

Geophysical Institute, Division A, University of Bergen, Bergen, Norway

J. MORISON

Polar Science Center, University of Washington, Seattle, Washington, 98105

B. A. FARRELLY AND E. A. S. SVENDSEN

Geophysical Institute, Division A, University of Bergen, Bergen, Norway

During September–October 1979 the Norwegian Remote Sensing Experiment was carried out in the marginal ice zone north of Svalbard. Convergence of the ice cover is correlated with along-ice edge winds with the ice to the right, while divergence occurs during off-ice winds or calm conditions. A wind-driven ice edge jet is observed. Wind-driven upwelling of the pycnocline of up to 7 m was present along the ice edge during a 10- to 15-m s easterly wind event. The upwelling is due to Ekman divergence at the ice edge, caused by higher wind stress over ice than over open water. The ice edge meanders with a scale of 20–40 km and sheds eddies with a scale of 5 to 15 km into the open water. This scale is of the same order as the Rossby radius of deformation. Eddies with the same scale are also seen in the conductivity, temperature, and depth observations. Conditions during the experiment were such that barotropic instabilities could have generated these eddies.

INTRODUCTION

The marginal ice zones (MIZ) are regions where temperate and polar climate systems interact, resulting in strong horizontal and vertical gradients in the atmosphere and the ocean. These gradients lead to mesoscale processes in the ocean, which affect the heat, salt, and momentum fluxes at the ice margin. It is therefore important to increase our understanding of these processes in order to model the air-ice-ocean system in the MIZ. Parameterization of these processes is also necessary in large scale modeling of the sea ice influence on the global climate system.

Few oceanographic studies from the region north of Svalbard are published. However, it is generally known that warm saline Atlantic water flows north in the West Spitsbergen Current and enters the Arctic Ocean as a subsurface current north of Svalbard. Along the coast of Greenland the cold, less saline East Greenland Current exports ice, polar water, and recirculated Atlantic water from the Arctic Ocean [*Coachman and Aagaard*, 1974; *Aagaard and Greisman*, 1975]. A description of the seasonal variation of the ice movement in the Greenland-Barents seas, including the region north of Svalbard, is summarized by *Vinje* [1977*a*]. *Buckley et al.* [1979] describe upwelling along the ice edge observed during a winter experiment north of Svalbard.

In order to gain a general picture of physical conditions in the MIZ north of Svalbard and, more specifically, to shed light on several important mesoscale processes at the ice edge, the Norwegian Remote Sensing Experiment (NORSEX) was carried out north of Svalbard in September and October 1979. This paper describes the oceanographic and ice studies carried out during the experiment. Subsequent to a description of the experimental program, attention will be devoted to three main areas. First, the general hydrographic conditions at the experimental site will be described and compared with those described by *Buckley et al.* [1978] for winter conditions at the ice edge. Second, the response of the ice to wind will be discussed with special attention to ice convergence and divergence and to an ice jet at the edge. Finally, the behavior of the upper ocean near the edge will be described with special attention to upwelling and eddies.

Paper number 2C1512.
0148-0227/83/002C-1512$05.00

DESCRIPTION OF EXPERIMENT

During the NORSEX experiment, which started September 18, 1979, the ice edge was located at about 82° N with a mean orientation of about 250°. The experimental region is shown in Figure 1 and was centered at approximately 81° 51'N, 10° E. It was partly over the Yermak Plateau with a depth of 800 m and partly over the southern slope of the plateau with depths down to 2500 m. A detailed bathymetric chart of this plateau has been published by *Sundvor et al.* [1982].

Conductivity, temperature, and depth (CTD) sections were carried out perpendicular and parallel to the ice edge, with station spacings of a few kilometers (Figure 2). A Neil Brown CTD (model MK3) was used for these measurements. Measurements of vertical shear were made with a profiling current system [*Morison*, 1980] at selected CTD stations. Continuous surface temperature measurements and bucket salinity samples were collected. Standard meteorological observations were taken every 3 hours.

At the start of the experiment, four drifting ice buoys, instrumented with atmospheric pressure and temperature sensors and using the ARGOS data transmission and positioning system, were parachuted onto the ice pack by a Norwegian Air Force P3 in a 200 by 200 km array, shown in Figure 1. Four drifting buoys using the ARGOS positioning system were de-

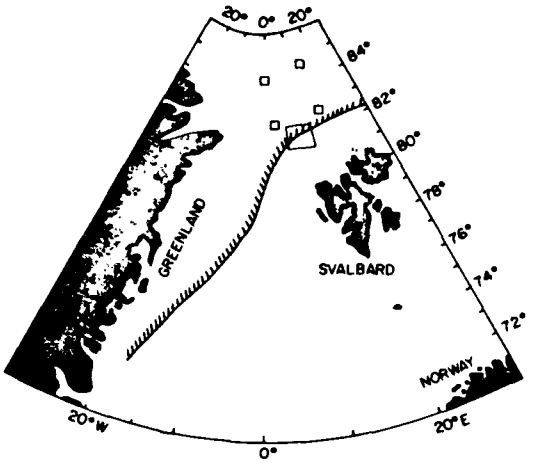

Fig. 1. Map with location of the experimental area (box) and air-dropped ARGOS buoys (small squares).

ployed from the ship 3–5 km in from the ice edge over a distance of 50 km along the edge. At one of these buoys, which was a toroid buoy, six Aanderaa current meters were suspended down to 300 m. This buoy, together with the drifting buoy located nearby, was recovered after about 10 days. All the others were left on the ice and continued to operate for 3 months, drifting downstream in the East Greenland Current. Four satellite-tracked surface drifters [*Audunson et al.*, 1981] were also deployed from the ship for a few days at a time. All buoy data were relayed to the Tromsø Satellite Telemetry Station and the ship twice daily. Data from the buoys along the ice edge enabled the movement of the ice edge to be followed and aided in the final adjustment of aircraft remote sensing flight tracks.

Remote sensing experiments were carried out, involving both ground truth measurements from the ship, and aircraft and satellite remote sensing. These experiments are described by *NORSEX Group* [1982] and *Svendsen et al.* [this issue]. Synthetic aperture radar (SAR) images of the ice edge region made from the NASA Convair 990 form an important element in this study.

HYDROGRAPHIC CONDITIONS

The vertical structure of the ocean in the ice-covered region of the experimental area can be described in terms of three main water masses, as defined by *Coachman and Aagaard* [1974]. First, the Arctic surface water extends down to 60 m and can be divided into two layers. A sharp pycnocline at about 20 m separates the fresh (32.35‰) mixed layer, with temperatures close to the freezing point (−1.70 C), from an intermediate layer below. This layer is nearly isothermal (−1.65 C) down to 60 m, with a strong halocline from 32.50‰ to 34.20‰. Second, the 'warm' Atlantic water core is at about 250 m with a temperature near 1.5°C and a salinity of 34.90‰. Finally, the Arctic bottom water extends from about 600 m to the bottom.

In the mixed layer off the ice edge, a weak horizontal frontal zone exists, where the fresh (32.50‰) and cold (−1.70 C) water which appears in the vicinity of the ice edge encounters more saline (33.40‰) and warmer (−0.5 C) water. The horizontal distance between the ice edge and the frontal zone varied from 10 to 60 km, primarily because of changes in the wind regimes and meandering of the frontal zone. A synoptic mapping of the surface temperature and salinity of the frontal zone by the R/V *Polarsirkel* on October 1 is shown in Figure 3, together with the main structure of the ice edge as derived from the SAR image (Figure 16) obtained the same day. The dark signature in the SAR image was identified as grease ice. At E1 the boundary of the grease ice appears to follow the same pattern as the frontal structure (Figure 3), thus suggesting that the boundary of the grease ice can be used as an indicator of the location of the front. The front is seen to meander with a scale of 20–40 km on this day of calm wind (3 m/s) and cold (−10°C) conditions. The changes of temperature and salinity across the front (20–40 km) are 1.0°C and 0.4‰ respectively, resulting in a density change of about $0.4\sigma_t$. A geostrophic flow calculation indicated no significant horizontal shear associated with this weak frontal zone.

The cold intermediate water (< −1.5°C) extends as a tongue from under the ice to about 60 km off the edge, as schematically shown in Figure 4. This figure is obtained by combining data from the region north of Svalbard collected in 1977 [*Buckley et al.*, 1978; A. Foldvik, personal communication, 1982] with data from this 1979 experiment. In the fall the intermediate cold layer insulates the ice from oceanic heat flux from the warmer

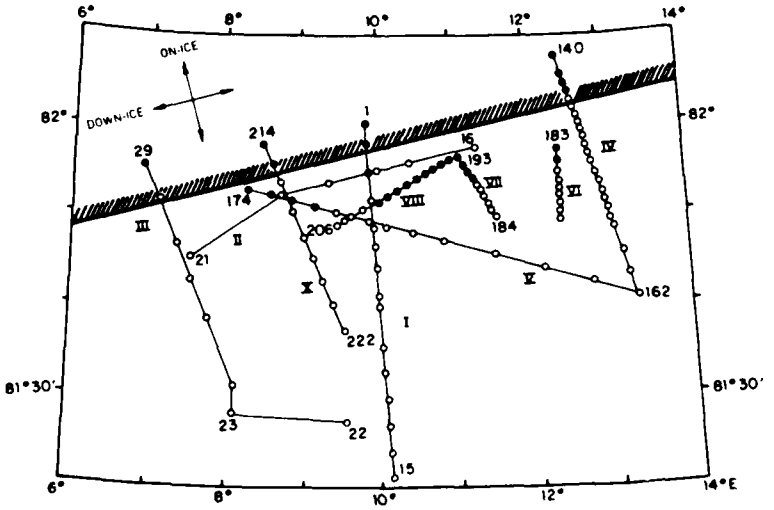

Fig. 2. Positions of the CTD sections I–X. Solid circles indicate stations in the ice, and open circles stations in the ocean. A mean ice edge location is also shown.

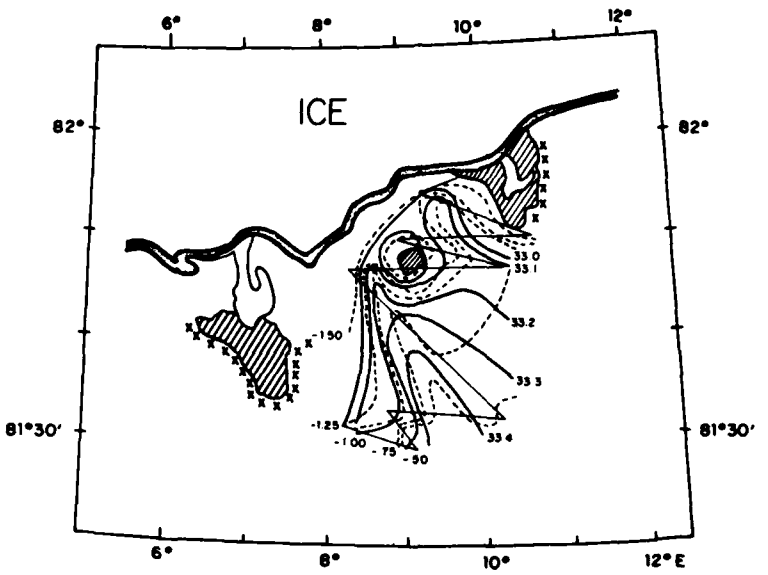

Fig. 3. Surface temperature and salinity mapped by R/V *Polarsirkel* on October 1. Thin lines indicate ship track, and hatched areas indicate grease ice. Crosses indicate the frontal boundary interpreted from the SAR image the same day.

Atlantic water [*Aagaard et al.*, 1981]. However, in winter, when the ice extends further south, the thermocline and pycnocline coincide near the ice edge, so that when entrainment occurs at the base of the mixed layer, heat is entrained and is available for inhibiting ice growth.

The Atlantic water is seen to enter the Arctic Basin along the shelf of Svalbard with the core at about 200 m (Figure 4). The 1.50°C isotherm indicates that water of Atlantic origin extends northward to about 82°. However, water of over 2°C at 200–300 m depth has been observed on the northern slope of the Yermak Plateau [*Morison and Burke*, 1981]. The temperature distribution in Figure 4 indicates that this water cannot be associated with the northward extension of the Atlantic water entering the Arctic Basin along the northern shelf of Svalbard. Rather, another branch of the Atlantic water must enter the Arctic Basin along the western slope of the Yermak Plateau.

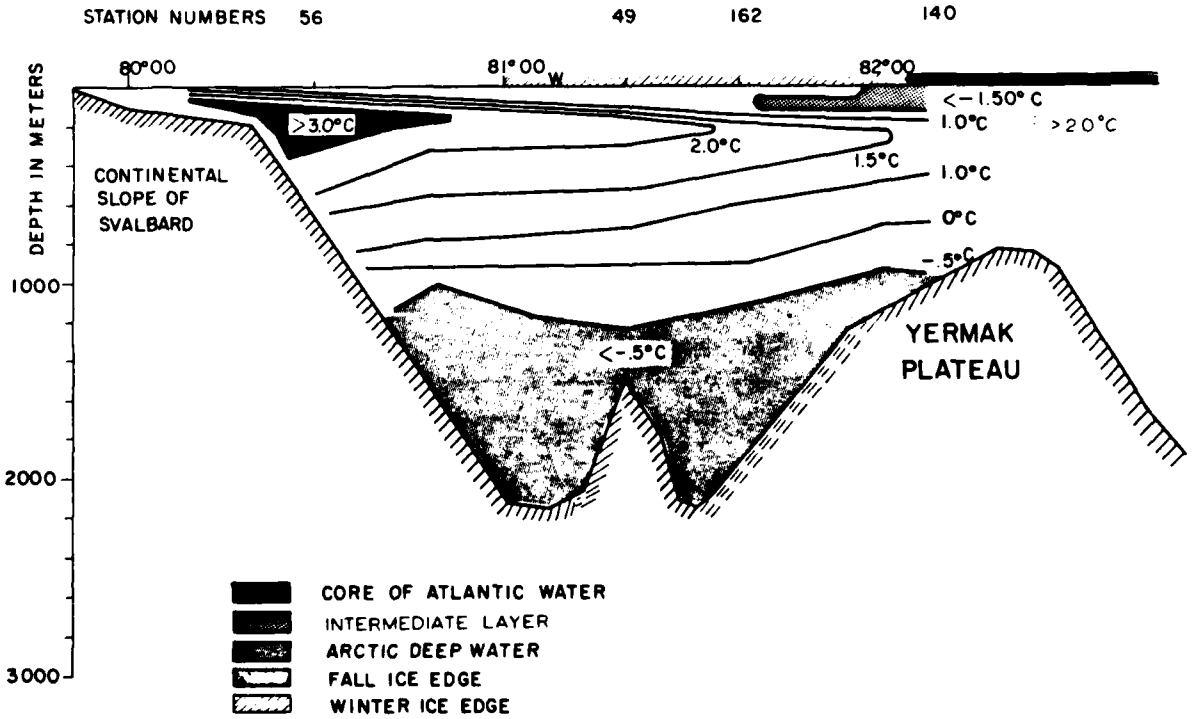

Fig. 4. Schematic temperature distribution of the water masses between Svalbard and the Yermak Plateau.

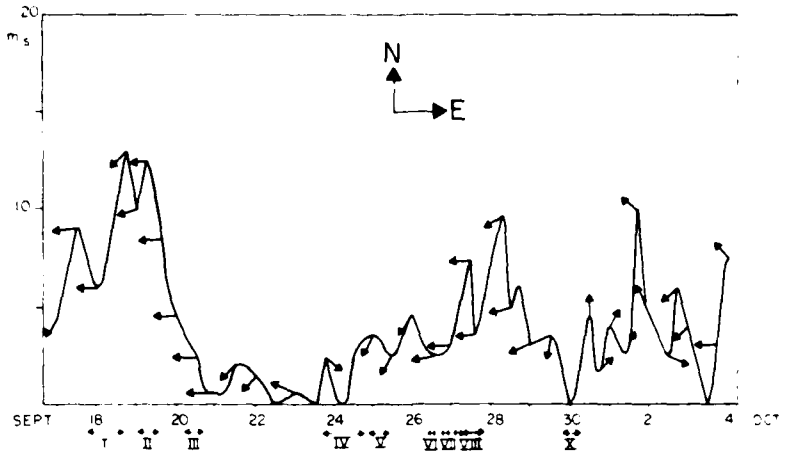

Fig. 5. Wind observed from R V *Polarsirkel* during the experiment. Arrows indicate direction. Inserted is the time the different CTD sections were made.

Ice Response to Wind

Comparisons of wind data with ice velocity and current velocity data illustrate two phenomena. First, winds parallel to the ice edge with the ice to the right when looking downwind (this direction will be referred to as 'down-ice'; see Figure 2) cause convergence of the ice and on-ice transport in the mixed layer. Second, when the wind blows down-ice, a jet in ice velocity occurs at the edge. The occurrence of these phenomena suggests that the ice in the ice edge region shows a greater response to the wind than does ice in the interior.

Ice Convergence and Divergence

Figure 5 shows the wind observed from the ship during the experiment. In general, the ship-measured wind agrees well with the wind derived from the surface atmospheric pressure maps [*Thorndike and Colony*, 1981] for our experimental region. The effect of wind on ice convergence can be seen by comparing the time series of wind with Figure 6, showing the shape of the ice edge on four different days, and Figure 7, which shows time series of ice convergence, wind velocity, ice velocity, and currents at the toroid buoy for the 9-day period the buoy was in operation. (Because of the strong coupling between the ice drift and the mixed layer current, a brief discussion of the current is included in this section.) Linear interpolation of buoy positions, from the array, extending 250 km in from the edge, were used to calculate the ice velocity field and the convergence-divergence variations. Absolute currents have been calculated by adding the ice drift. A low-pass Butterworth filter [*Roberts and Roberts*, 1978] with a cutoff of 35 hours was applied to the ice and current velocity in order to eliminate inertial and tidal motion. The wind was also filtered with a 35-hour cutoff.

As shown in Figure 5, a strong easterly wind blew on September 18 and 19, and Figure 6*a* shows that the ice edge was straight and displaced the maximum distance north. After the strong wind event, calm conditions prevailed, and Figure 7 shows the ice to start diverging on September 22. Ice and water velocities were low. On September 24, weak off-ice winds developed, and the ice divergence reached a maximum of 4% day. The current patterns measured at the toroid also show a weak component of off-ice transport in the mixed layer during this period. Figure 8*a* shows the average of all the velocity profiles measured relative to 15 m with the profiling current meter system on September 24. Most of the profiles were obtained in open water. Also inserted are the 35-hour filtered absolute ice drift and currents at the toroid buoy measured on September 24. Both sets of data show a weak off-ice velocity component in the mixed layer and a component down-ice. Figure 6*b* shows that the ice edge, as traced by the ship on September 25 and early on September 26, had moved south and meandered with a scale of 20 to 40 km. The edge at this time was very loose.

After September 25 (Figure 7), the wind increased and turned clockwise until it had an on-ice component on September

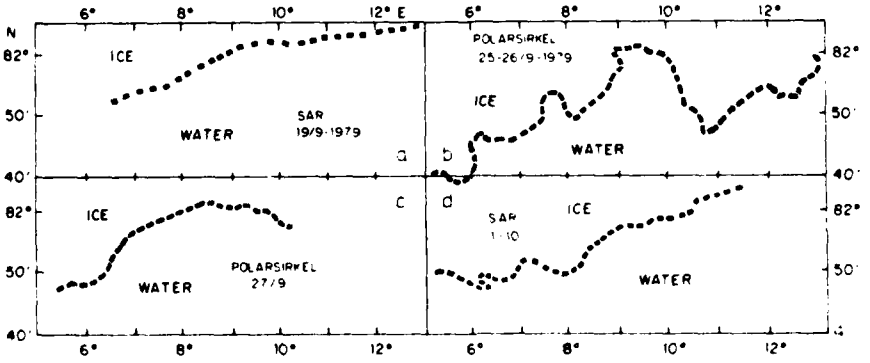

Fig. 6. Ice edge mapping during the experiment

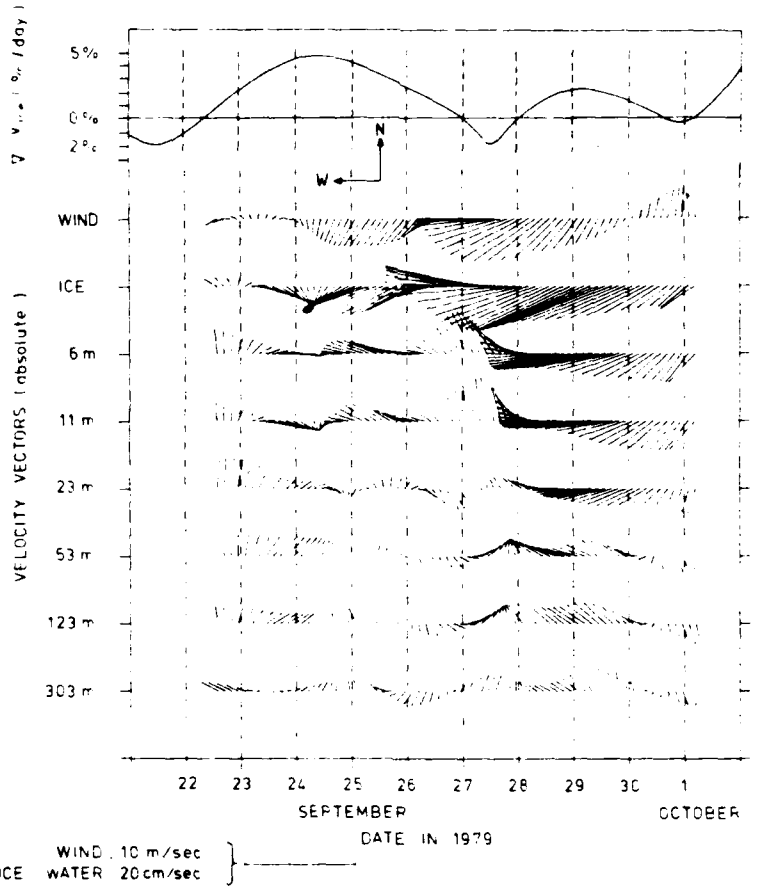

Fig. 7. Divergence of the ice calculated from six ice drifting buoys, ship-measured wind and ice drift and absolute current from the drifting toroid buoy. All low-pass filtered with 35-hour cutoff.

26–27. This resulted in a decrease in the divergence until the maximum convergence of 2% day was reached on September 27. Figure 6c shows the ice edge on September 27 to have moved northward and become straighter. The ice drift vector was deflected to the right of the wind with a further deflection of the current in the mixed layer. Figure 8b shows the average of all the velocity profiles made in open water and in the ice near the ice edge on September 26, along with the current meter and the ice velocity data and the drift of a surface drifting ARGOS buoy in the open water. All the velocity data show the

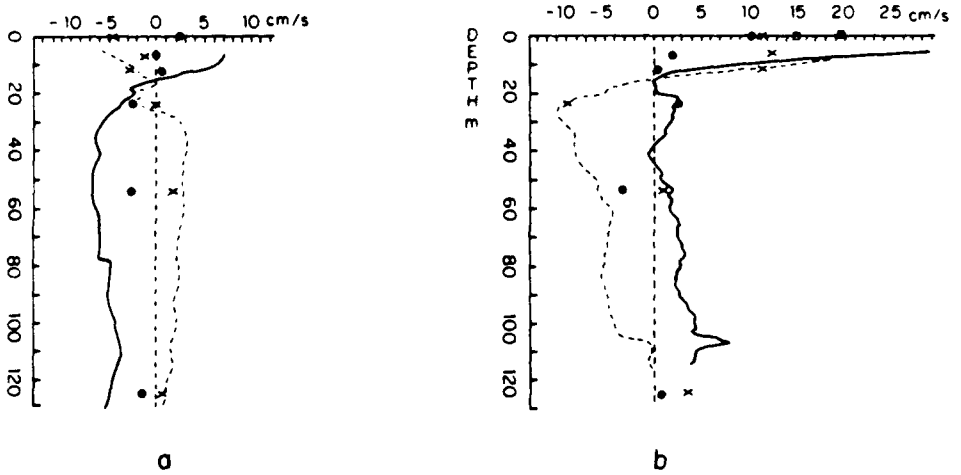

Fig. 8. Average velocity profiles relative to 15 m on (a) September 24 and (b) September 26. Solid lines positive down-ice, dashed lines on-ice. Current from the toroid buoy (circles down-ice, crosses on-ice) is shown in comparison. Also inserted in Figure 8b is surface drift from the ARGOS buoy in the open water on September 26 (solid square down-ice, open square on-ice).

Fig. 9. Jet Propulsion Laboratory synthetic aperture radar (1.215 GHz) image of the marginal ice zone on September 19, 1979 [after *NORSEX Group*, 1982].

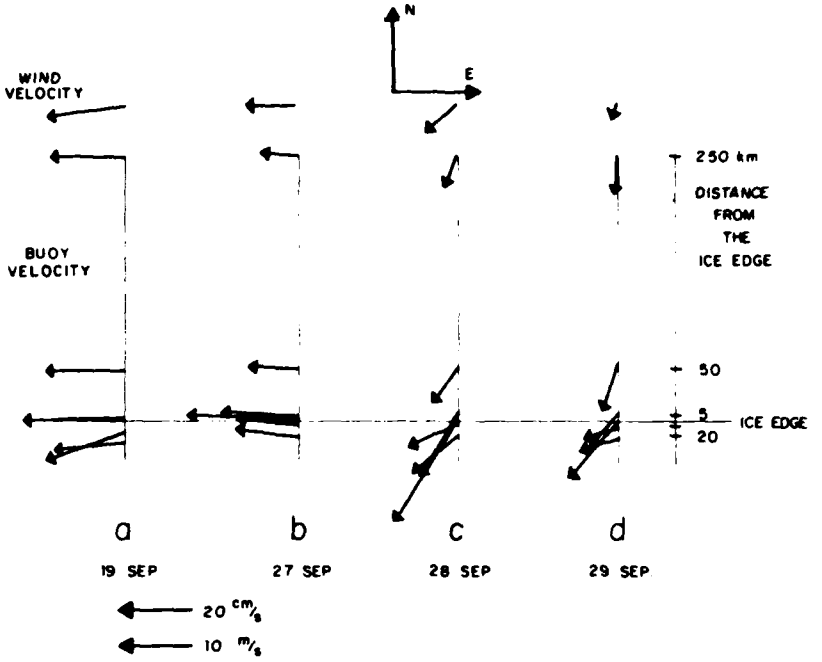

Fig. 10. Daily average ice drift and surface current from the ARGOS drifting buoys, and ship-measured wind on (*a*) September 19, (*b*) September 26, (*c*) September 27, and (*d*) September 28.

same pattern: the mixed layer current and surface drift components were toward the ice and down-ice. The mixed layer current and surface drift were much larger than those measured during calmer wind conditions on September 24. (The profiles show larger currents than the other data in the mixed layer, especially at depths less than 10 m. This is probably due to disturbance of the flow by the ship.)

On September 28 the wind turned off-ice and decreased. The divergence (Figure 7) again became positive. The ice converged slightly on September 30 because of a weak southerly wind. The ice edge contour for October 1, shown in Figure 6*d*, was at about the middle of its north-south range and displayed meandering.

These records demonstrate that down-ice wind causes convergence of the ice, straightening of the ice edge, and on-ice transport in the mixed layer. Furthermore, off-ice wind and calm conditions cause divergence and meandering of the ice edge. In order for on-ice or down-ice winds to cause convergence (or for off-ice or up-ice winds to cause divergence), the ice in the ice edge region must respond more to the wind than does ice in the interior. Mechanisms which might cause the stronger ice response to wind will be discussed further below.

Ice Edge Jet

There are a number of indications that under conditions of down-ice winds, the ice velocity is a maximum at the ice edge. During the peak wind event on September 19, the ice edge, shown in the SAR image of Figure 9, was straight. The numerous ice plumes shown in the figure, trailing off from the ice edge to the east, as well as the northeastward striking ice features in from the edge, suggest that the first 10 to 15 km of the ice cover was moving faster than the water off the edge and the ice cover further in. This structure in the SAR image can be interpreted as an ice edge jet and is verified by contemporaneous data from the drifting buoys on the ice and in the surface water (upper 0.5 m) off the edge. The average buoy velocities for September 19 are shown in Figure 10*a*. The velocity along the ice edge, 5 km in from the edge, is about 0.27 m/s, decreasing to about 0.20 m/s at 50 to 250 km in from the edge. The speed of the surface layer off the ice edge is also of the order of 0.20 m/s. Other examples of similar profiles are seen in Figures 10*b–d* for September 27–29 and are associated with the second major down-ice wind event. Again, maximum ice drift is observed at the ice edge. During this period an ARGOS buoy was located on a multiyear ice floe 50 m in from the ice edge. This buoy achieved a maximum speed of 0.30 m/s (Figures 10*b* and 10*c*), 0.10 m/s higher than the speed 5 km further in, suggesting that the strongest ice velocity gradient occurs in the outer 5 km.

Estimates of wind drift coefficients provide quantitative evidence of the increased coupling between ice and wind at the ice edge and suggest that the ice edge jet is a ubiquitous, wind-driven feature. The drift coefficient A is a complex constant which, when multiplied by the deviation of the wind velocity from the mean wind, produces a least squares fit to the deviation of ice velocity from the mean ice velocity. The drift coefficient was calculated, using the statistical method of *Thorndike and Colony* [1982], for the six ice drifting buoys (Figure 11). The buoy drifts over a 40-day period were used along with geostrophic winds from the Arctic Ocean Buoy Program [*Thorndike and Colony*, 1981].

Table 1 lists the drift coefficients computed for the six buoy records from September 17 to October 27 1979. Figure 12 shows the average values of $|A|$ determined by combining data from the pairs of buoys: at the ice edge, 50 km in from the edge, and 250 km in from the edge. The coefficients increase in magnitude as one nears the ice edge, from about 0.9% in the interior to 1.2% at 50 km from the edge, to 1.9% at the edge. The turning angles also increase as one nears the ice edge. The coefficients for the interior are slightly greater than the 0.8% value obtained by Thorndike and Colony for yearly average

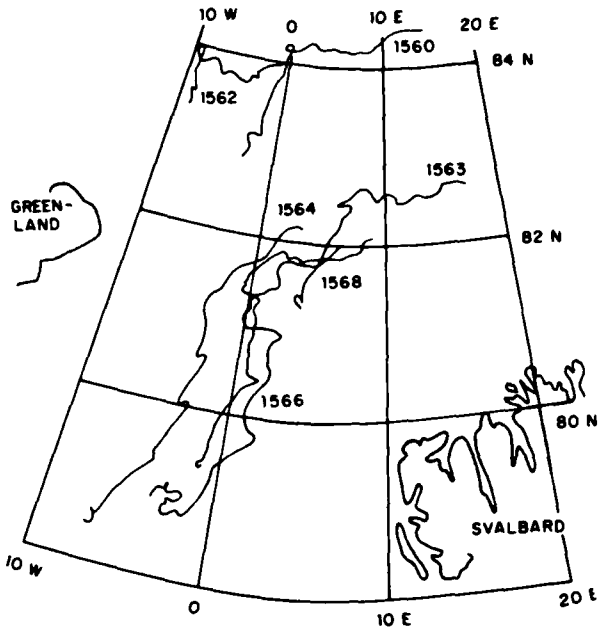

Fig. 11. Drift pattern of the ice drifting buoy array over a 40-day period, from September 17 to October 27.

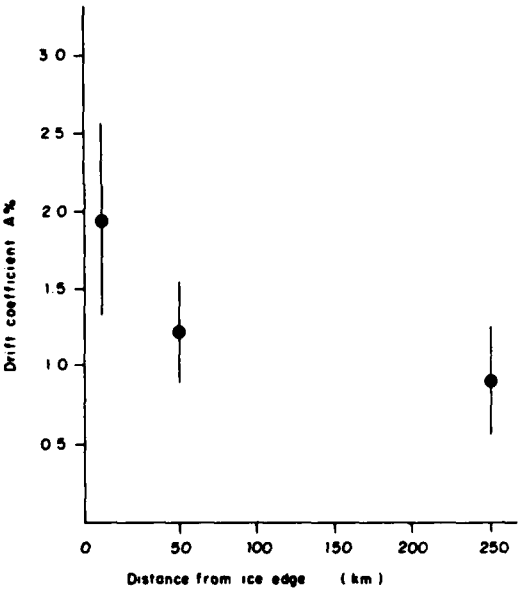

Fig. 12. Drift coefficient $|A|$ as a function of distance from the ice edge. A 95% confidence interval is inserted.

values in the interior pack ice, and are slightly less than the 1.05% value they obtained for the summer conditions in the pack. However, both these values are within the confidence interval (Table 1).

On the average the wind drift accounts for about 51% of the variance in the ice drift. This is substantially less than the value of 86% found by *Thorndike and Colony* [1982] for the interior pack ice. This, in turn, implies that there is higher variability in the ocean currents in the experimental region than in the Arctic Ocean as a whole.

The larger drift coefficient tells us that the coupling between the wind and the ice drift is consistently greater in the ice edge region than further in. Moreover, the wind was predominantly easterly to northeasterly, suggesting that the ice edge jet in this region north and northwest of Svalbard is a wind-driven feature. The stronger coupling between wind and ice drift, as demonstrated by the large drift coefficient in the ice edge region, is consistent with the tendency described above for the ice to converge and diverge under varying wind conditions. It should be pointed out that, as shown by *Vinje* [1977*b*] and *Paquette* [1982], ice edge jets found further south in the East Greenland Current may also be associated with ocean jets due to strong frontal shear.

In addition, *Roed and O'Brien* [1981] obtain an ice edge jet of the order of 0.5 m/s in an analytical model simply by balancing the Coriolis force and the internal ice pressure. However, our ice drifting buoys revealed no jet of such a magnitude under calm conditions, suggesting that this model is too simple.

There are several potential reasons for the stronger coupling between the wind and ice drift near the ice edge. The ice near the edge may be freer to respond because of a decrease in the effect of the internal ice stress. The wind stress may be larger at the edge because of an increase in surface roughness. There is an added coupling of the ice to the wind near the ice edge due to the effects of wind wave radiation pressure. Finally, it is possible that the ice velocity jet is enhanced by an ocean current in the mixed layer associated with wind-driven upwelling.

Since there is a free boundary along the ice edge, ice in the outer ice edge region may obey the free ice drift law, while further in, the internal ice stress will become more important and retard ice motion. Evidence of this is seen in the comparison of the rotary spectra for the two buoys 1562 and 1566 deployed 250 and 5 km in from the ice edge, respectively

TABLE 1. Drift Coefficients $|A|$ for the Six Ice Drifting Buoys, Corresponding Turning Angles, Percentage of Variance Accounted for by the Wind, 95% Confidence Interval, and Initial Distances From the Ice Edge

Buoy	Coefficient $\|A\|$	Turning Angle	Percentage of Variance Accounted for by Wind	95% Confidence Interval	Initial Distance From Ice Edge, km
1560	0.0093	−9	48	0.0045	250
1562	0.0090	0	39	0.0053	250
1563	0.0110	−16	63	0.0039	50
1564	0.0140	−10	58	0.0053	50
1566	0.0210	−23	52	0.0094	5
1568	0.0170	−20	51	0.0079	5

(Figure 13). The spectra were estimated using the maximum entropy method based on an algorithm of *Smylie et al.* [1973]. Mean and trend were removed before estimation. Positive frequencies represent anticlockwise rotation. The highest spectral density, at −2 cpd, is clearly seen for the ice edge buoy 1566. According to *Kowalik and Untersteiner* [1978], the M2 tidal motion in the region is essentially linear, requiring an equal contribution at positive and negative frequencies in the rotary spectra. The predominance of clockwise rotation at −2 cpd for the ice edge buoy is then mainly due to the presence of inertial motion. The peak at −2 cpd is absent at the interior buoy. This suggests that the damping of inertial motion by internal ice stress is much less at the edge than in the interior.

The wind stress may be larger in the ice edge region because of the increased surface roughness. Aerial photographs obtained from the remote sensing flights together with surface observations show that in the first 10 km the ice floe size varied from 0.5 m up to 25 m, while in the next 10–15 km the floe size varied from 25 to 50 m. From 25 km inward, the maximum floe size was several hundred meters. Measurements of the drag coefficient in the Gulf of Saint Lawrence by eddy correlation techniques over broken and small ice floes (similar to the floes in our ice edge region) have yielded a mean drag coefficient at 10 m of 3.1×10^{-3}, with a maximum value of 4.0×10^{-3} under unstable conditions [*Smith et al.*, 1970]. *Macklin* [this issue] also obtained a drag coefficient of 3.1×10^{-3} over fractured and rafted ice with floe sizes of 10 to 20 m in the Bering Sea. These values exceed those for interior pack ice of about 2.0×10^{-3} estimated during the Arctic Ice Dynamics Joint Experiment [*Leavitt*, 1980] and the value for open water of 1.5×10^{-3} for moderate wind conditions [*Amorocho and DeVries*, 1980]. Therefore our ice floe size distribution suggests that the drag coefficient should have a maximum value at the ice edge and decrease inward.

The effect of increased drag and decreased internal ice stress on the drift coefficient can be evaluated quantitatively by using the crude assumption that the wind stress on the ice is balanced solely by the water stress [*Thorndike and Colony*, 1982]. The magnitude of the drift coefficient can be approximated by

$$|A| = (\rho_a c_a / \rho_w c_w)^{1/2} \quad (1)$$

where c_a is the geostrophic drag coefficient for the wind stress over ice, c_w the geostrophic drag coefficient for the water stress, ρ_a the air density, and ρ_w the water density.

Using parameters representative of pack ice conditions from *Albright* [1980] and *McPhee* [1980] yields a value for c_a of 0.9×10^{-3}. Combining this with *McPhee*'s [1980] estimate of c_w equal to 5.5×10^{-3} yields $|A|$ equal to 1.5% [*Thorndike and Colony*, 1982]. In order to increase the drift coefficient to the value of 1.9% found at the ice edge, the ratio of c_a to c_w must be increased by a factor of 1.6. If the largest estimate of the surface drag coefficient from *Smith et al.* [1970], 4.0×10^{-3}, is used, the resulting value for c_a at the ice edge is about 1.4×10^{-3}. This gives a drift coefficient of 1.8%, approaching the observed value. However, the retention of c_w at the pack ice value is unreasonable as c_w increases near the ice edge because of the prevalence of smaller ice floes. This has been observed for similar ice conditions in the Gulf of Saint Lawrence by *Johannessen* [1970] and in the Bering Sea by *Pease et al.* [this issue]. Thus an increase in wind drag and decrease in internal ice stress in the ice edge region are not sufficient by themselves to explain the higher drift coefficient at the ice edge.

A third explanation which can increase the coupling of wind and ice velocity at the edge is the effect of wave radiation pressure. *Wadhams* [1981] suggested that wave radiation pressure due to swell can be a significant factor in compaction of the ice edge. The importance of wind wave radiation stress on bands in the ice edge region has been studied by *Martin et al.* [this issue] for the Bering Sea. They calculate that the relative magnitude of the wind wave radiation stress on the upwind side of the bands is about 30% of the water stress. However, during the NORSEX experiment, with prevailing easterly winds, no bands were observed, and the fetch between ice floes remained limited. Therefore the relative importance of wind wave radiaion stress in the momentum balance was probably small during NORSEX, at least as far as ice drift parallel to the edge is concerned. However, the importance with regard to convergence at the edge due to on-ice winds may be considerable.

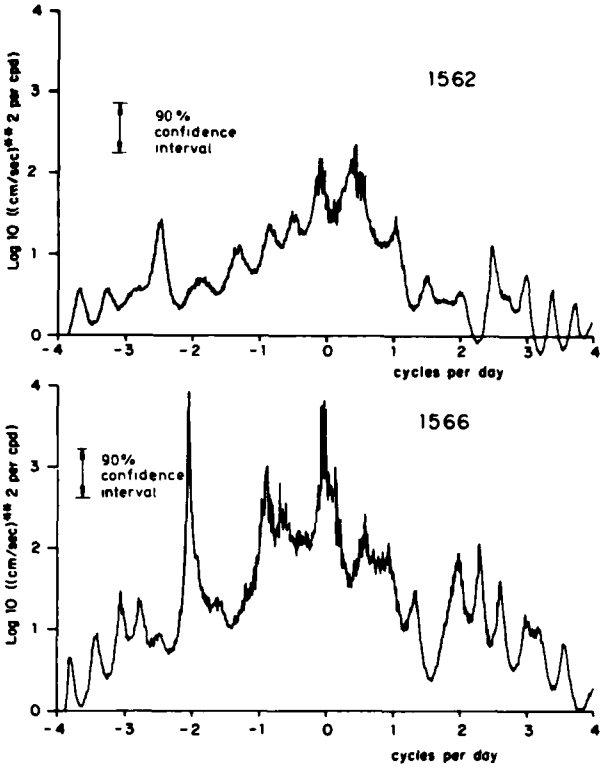

Fig. 13. Rotary spectra of an ice edge buoy, 1566, and an interior buoy, 1562, over a 40-day period from September 17 to October 27. A 95% confidence interval is inserted.

A fourth explanation for the ice edge jet can be that it is enhanced by an ocean current near the ice edge which is associated with wind-driven upwelling. This idea is discussed further in the next section.

Upper Ocean Response

The behavior of the upper ocean during the experiment can be characterized by upwelling events and the generation of eddies at the ice edge.

Upwelling

The observations of upwelling during NORSEX must be examined in comparison with other observations and models of the phenomena. Upwelling along the ice edge was first observed by *Buckley et al.* [1979] during a winter experiment north of Svalbard. Their experiment was inspired by the theo-

retical study of upwelling by *Gammelsrød et al.* [1975], in which the response of a homogeneous ocean was modeled. The model employs the assumption of an ice sheet unable to move horizontally. The work has been extended by *Clarke* [1978] for a stratified ocean. *Niebauer* [1982] developed a numerical model of the wind response of a stratified shallow ocean near an ice edge, which also employs the assumption of a nonmoving ice sheet. In these models the ice sheet isolates the ocean from wind stress, so that up-ice winds cause divergence of Ekman transport and, consequently, upwelling at the ice edge. The observations of *Buckley et al.* [1979] and, more recently, *Alexander and Niebauer* [1981] seem to fit this general picture. A model recently developed by *Røed and O'Brien* [this issue] yields the coupled response of the ice and a two-layer ocean to wind. In this case the ice is allowed to move and to display internal ice stress. Their results are the opposite of those found in the other theoretical studies. Because the drag coefficient over ice is larger than that over water (at least for neutral stability), they find that allowing the ice to move (as it obviously does) in response to wind produces upwelling at the edge when the wind blows down-ice.

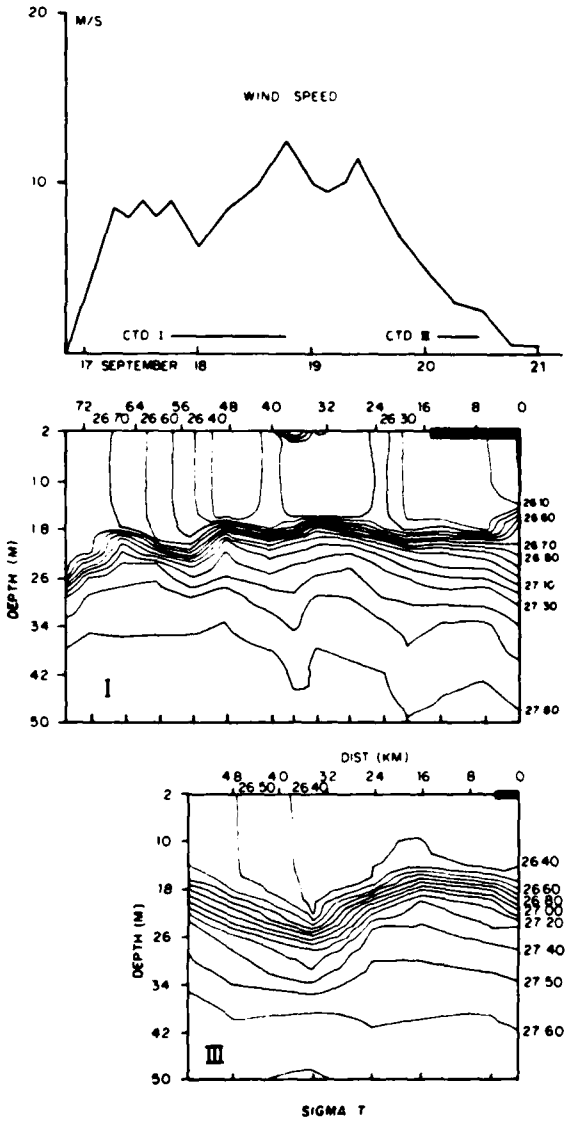

Fig. 14. Density structure from CTD sections I and III, and wind speed during the first major easterly wind event. Stations indicated at the bottom of the sections.

Evidence of upwelling during NORSEX appears in records made during the two major easterly wind events. As discussed earlier, Figure 5 shows that a strong easterly wind event occurred on September 18–19. Figure 14 shows the wind speed for this period along with two CTD sections, I and III, carried out perpendicular to the ice edge on September 18 and 20. Section I was 40 km upstream of section III. This distance corresponds well with the average surface current (see Figure 10*a*) of 0.20 m/s, enabling us to follow approximately the Lagrangian development of the upwelling [for example, *Johannessen et al.*, 1977]. Comparison of the two sections indicates that the pycnocline at the ice edge rose during this wind event. For example, the maximum vertical displacement of the $26.4\sigma_t$ isopycnal was 6 m in about 2 days. The deeper isopycnals were also lifted in the ice edge region. For example, the $26.7\sigma_t$ isopycnal moved upward about 7 m. Given the ice edge orientation shown in Figure 9, the difference in ice edge position in the two CTD sections represents an average northward displacement of the ice edge of about 15 km during this period.

As shown in the section on ice response, the ice near the edge is free to move and appears to act as if in a state of free drift. The assumptions used in the model of *Røed and O'Brien* [this issue] where the internal ice stress is neglected are appropriate for these conditions, while the assumptions of a nonmoving ice sheet by *Gammelsrød et al.* [1975], *Clarke* [1978], and *Niebauer* [1982] are not.

The observations can also be compared quantitatively to the model of *Røed and O'Brien* [this issue]. Their analytical solution for the mixed layer depth of the two-layer ocean is

$$h(x, t) = H - (H\gamma a u_0 t/2f^2L) \exp\left[-(x - u_0 t)/L\right] \qquad (2)$$

where $\gamma = C_w/H$, $a = \rho_w C_w/\rho_i D$, and $L = f^{-1}(g'H)^{1/2}$. H is the equilibrium mixed layer depth; C_w is the ice-water drag coefficient; ρ_w is the water density; ρ_i is the ice density; D is the mean ice thickness; u_0 is the on-ice velocity; f is the Coriolis parameter; L is the deformation radius; g' is reduced gravity; and x is the position measured positive in the on-ice direction from an initial position $x_0 = 0$. The value for u_0 is given by

$$u_0 = [\tau/\rho_i D f]\,[1 + (a/f)^2]^{-1} \qquad (3)$$

and τ is the wind stress on the ice. Their model sets the wind stress over open water equal to zero for simplicity. By applying data from our region with a 10-m/s easterly wind blowing parallel to the ice edge for 1 day, their model predicts an upwelling of about 18 m. In addition, the ice edge is displaced northward about 12 km. However, if the wind stress over open water is prescribed, this upwelling will be reduced to 6 m (L. P. Røed, personal communication, 1982). It was also found that increasing their ice-water drag coefficient by a factor of 10 only increased the upwelling from about 18 to 24 m. Their model is thereby relatively insensitive to an accurate value for the ice-water drag coefficient. The quantitative agreement between their analytical model and the NORSEX observations supports the interpretation that the easterly wind event from September 18 to September 20 was strong enough to generate upwelling. During the second major easterly wind event from September 27 to September 29, comparison of CTD sections IV and X indicated that a weak upwelling, of the order of 3 m, took place in the ice edge region (Figure 15). This is also in quantitative

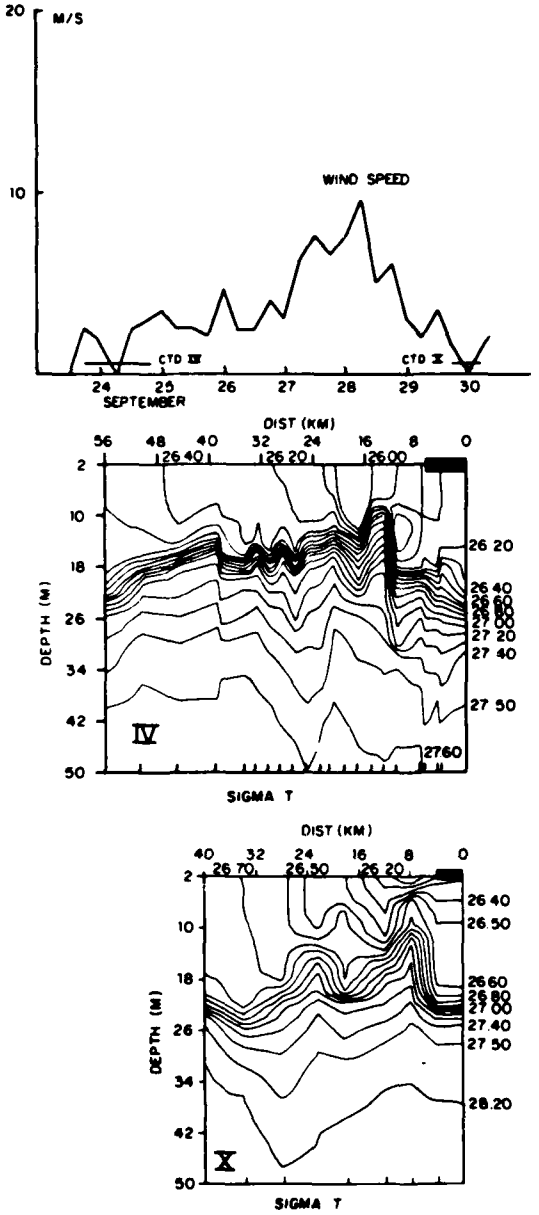

Fig. 15. Density structure from CTD sections IV and X, and wind speed during the second major easterly wind event. Stations indicated at the bottom of the sections.

agreement with the model by *Røed and O'Brien* [this issue]. However, the interpretation of upwelling in this figure is complicated by the presence of eddies as discussed in the next section. This complication was not present in CTD sections I and III used in the discussion of the first upwelling event. It is also noted that the isopycnals in section IV (Figure 15) are elevated near the ice edge, and one can speculate that this elevation also was caused by the first major wind event, thus implying that the decay time of the upwelling at least is of the order of a few days.

Røed and O'Brien [this issue] also predict upwelling under calm conditions driven by an ice edge jet which is assumed to be caused by internal ice pressure in balance with the Coriolis force. As was mentioned earlier, our data revealed no such jet under calm conditions, and we therefore reject this upwelling mechanism.

The obvious question that arises is, why do the upwelling observations of *Buckley et al.* [1979] and *Alexander and Niebauer* [1981] agree with the models of *Gammelsrød et al.* [1975], *Clarke* [1978], and *Niebauer* [1982], while the NORSEX observations favor the upwelling model of *Røed and O'Brien* [this issue]? The assumption of a nonmoving ice sheet is poor, and given this, the upwelling mechanism described in the earlier models is inappropriate. Is there another physical explanation for the observations of upwelling with up-ice wind? The magnitude of wind stress over water can be larger than that over ice, and thus produce upwelling for up-ice winds, if the stratification in the atmospheric boundary layer is unstable. For example, *Buckley et al.* [1979] reported an air temperature of $-25°C$ a few kilometers off the ice edge. Extrapolating for such conditions from model data by R. A. Brown (personal communication, 1982) yields geostrophic drag coefficients for the open water of about 1.6×10^{-3} for a wind speed of 10 m/s. Assuming that the ice temperature is equal to the air temperature, Brown's model suggests that the geostrophic drag coefficient over ice is about 1.4×10^{-3} for 10-m drag coefficients of 3.1×10^{-3}. This goes some way toward explaining the observations of *Buckley et al.* [1979] and possibly the observations of *Alexander and Niebauer* [1981].

Geostrophy requires the presence of an ocean current at the ice edge whenever there is upwelling at the edge. However, the strength of this current depends on the width and the intensity of the upwelling. For example, the upwelling seen in CTD section III (Figure 14) was wide (30 km, nearly an order of magnitude larger than the deformation radius), and no significant geostrophic current near the ice edge was calculated. (The geostrophic velocities were calculated in relation to 200 m because direct current measurements indicated that this was a level of weak motion.) On the other hand, CTD section X obtained after the second major down-ice wind event shows the presence of a narrow region of raised pycnoclines near the ice edge (upwelling and eddies) with associated geostrophic velocities of up to 0.20 m/s (Figure 17). Similar velocities near the ice edge were also calculated for CTD section IV.

Mesoscale Eddies

Eddies at the ice edge in the East Greenland Current have been seen in visual and IR imagery [*Vinje*, 1977*b*; *Wadhams*, 1981], and in sound velocity profiles [*Wadhams*, 1978]. *Wadhams and Squire* [this issue] describe the behavior of an eddy in this region in terms of ice drift and CTD measurements. This eddy is of the order of 60 km across, and using the results of *Griffiths and Linden* [1982], Wadhams and Squire claim that the eddy is due to a baroclinic instability.

Observations of eddies were also made during NORSEX. They are much smaller than those in the east Greenland Current and probably depend to a greater degree on barotropic instability for their generation. Figure 16 shows the SAR image for October 1. Distinct surface features of four eddies, E1–E4, with horizontal scales of 5–15 km can be seen in the image. The eddies, E1–E3, extend out from the ice edge with a cyclonic rotation. As has previously been mentioned, the dark signature indicates the presence of grease ice. The circular shape and the size (5 km) of the patch, E4, suggest that it is a manifestation of an ocean eddy off the ice edge. The map of the frontal structure shown in Figure 3 suggests that the eddy is embedded in the frontal zone.

Fig. 16. Jet Propulsion Laboratory synthetic aperture radar (1.215 GHz) image of the marginal ice zone on October 1, 1979 [after *NORSEX Group*, 1982].

deformation to the horizontal length scale of the flow, and δ, the fraction of the total fluid depth occupied by the layer inside the front. By applying data from our experimental region, where $\delta = 0.02$ and $\theta = 0.013$, their results suggest that the instabilities are barotropic.

Griffiths and Linden [1982] also studied instabilities in density-driven boundary currents. They concluded that, provided the current width is comparable to the baroclinic Rossby radius of deformation,

$$L = (g'H)^{1/2}/f$$

the instability will be barotropic. On the other hand, if L_s is much bigger than L, the instability is likely to be baroclinic. In the NORSEX region, where L is approximately 3.5 km, L_s is approximately equal to L. Therefore the eddies observed were probably generated by barotropic instabilities. *Wadhams and Squire* [this issue] also use these results, and, since L_s is approximately 200 km and L is 8 km for their case, they conclude that instabilities in the East Greenland Current are baroclinic.

SUMMARY

Interpretation of the NORSEX observations, in the MIZ north of Svalbard for the early fall, leads to the following conclusions:

During early fall, the ice edge is north of the southern limit of a cold intermediate layer of water beneath the mixed layer. This intermediate layer insulates the ice from the underlying 'warm' Atlantic water. Comparison with data taken in the winter of 1977 indicates that this insulating layer is not present in the ice edge region during winter.

During moderate to strong wind events, with the wind blowing down-ice, the ice edge is straight because of ice convergence, while during off-ice winds or calm conditions, the ice diverges and meanders with a scale of 20 to 40 km. Also, a down-ice jet in ice velocity is observed at the edge when the wind blows down-ice. These facts suggest that the response of the ice to the wind is greatest at the ice edge. There are four explanations suggested for this. The two most important explanations are the reduction of internal ice stress near the edge, allowing free ice drift and the increase in wind stress near the edge because the small floe size there increases the surface roughness. In addition, the ocean current associated with the upwelling and the wind wave radiation pressure may influence the ice velocity.

Upwelling of the pycnocline of about 7 m was observed during the major (up to 15 m/s) easterly wind event. The upwelling is associated with Ekman divergence at the ice edge due to the presence of a larger wind stress over the ice than over the open water. These observations are in quantitative agreement with the ice edge upwelling model by *Røed and O'Brien* [this issue].

Eddies are present along the ice edge with scales of 10 to 15 km, of the order of the internal Rossby radius of deformation. Our observations reveal that both horizontal and vertical shears are present. Application of *Griffiths and Linden*'s [1981, 1982] laboratory results to our data suggests that the eddies are generated by barotropic instability

Acknowledgments. The NORSEX program reported in this paper was funded by the University of Bergen, Norway; Office of Naval Research grant 0014-80-9-0063 to the University of Bergen and grant 00N-00014-79-C-00240 to the University of Washington, Seattle, Washington; the U.S. National Aeronautic and Space Administration; the Royal Norwegian Council for Scientific and Industrial Research, Space Activity Division; and the NATO Scientific Affairs Division, grant 9-4-02-SEG.19. The support from the Royal Norwegian Air Force in dropping the ice drifting buoys is appreciated. The first two authors spent a year at Naval Postgraduate School, Monterey, where much of this manuscript was prepared. They wish to express their appreciation to their colleagues and to those who made their stay possible.

REFERENCES

Aagaard, K., and P. Greisman, Toward new mass and heat budgets for the Arctic Ocean, *J. Geophys. Res.*, *80*, 3821–3827, 1975.

Aagaard, K., L. K. Coachman, and E. Carmack, On the halocline of the Arctic Ocean, *Deep Sea Res., Part A*, *28*(6), 529–545, 1981.

Albright, M., Geostrophic wind calculation for AIDJEX, in *Sea Ice Processes and Models*, edited by R. S. Pritchard, pp. 402–410, University of Washington Press, Seattle, Wash., 1980.

Alexander, V., and H. J. Niebauer, Oceanography of the eastern Bering Sea ice-edge zone in spring, *Limnol. Oceanogr.*, *26*(6), 1111–1125, 1981.

Amorocho, J., and J. J. DeVries, A new evaluation of the wind stress coefficient over water surfaces, *J. Geophys. Res.*, *85*(C1), 433–442, 1980.

Audunson, T., V. Dalen, K. Krogstad, H. N. Lid, and P. Steinbakken, Some observations of ocean fronts, waves and current in the surface along the Norwegian coast from satellite images and drifting buoys, in *Proceedings From the Norwegian Coastal Current Symposium, Geilo, 9–12 September 1980*, University of Bergen, Bergen, Norway, 1981.

Buckley, J. R., A. Evjen, T. Gammelsrød, O. M. Johannessen, L. P. Røed, and H. Røyset, Hydrographic observations from the cruise north of Spitsbergen, December 1977, *Rep. 48*, Geophys. Inst., Univ. of Bergen, Bergen, Norway, July 1978.

Buckley, J. R., T. Gammelsrød, J. A. Johannessen, O. M. Johannessen, and L. P. Røed, Upwelling: Oceanic structure at the edge of the Arctic ice pack in winter, *Science*, *203*, 165–167, 1979.

Clarke, A. J., On wind driven quasi geostrophic water movement at fast ice edges, *Deep Sea Res.*, *25*, 41–51, 1978.

Coachman, L. K., and K. Aagaard, Physical oceanography of Arctic and Subarctic seas, in *Marine Geology and Oceanography of the Arctic Seas*, edited by Y. Herman, pp. 1–72, Springer, New York, 1974.

Gammelsrød, T. M., Mork, and L. P. Røed, Upwelling possibilities at an ice edge, homogeneous model, *Mar. Sci. Commun.*, *1*, 115–145, 1975.

Griffiths, R. W., and P. F. Linden, The stability of vortices in a rotating, stratified fluid, *J. Fluid Mech.*, *105*, 283–316, 1981.

Griffiths, R. W., and P. F. Linden, Laboratory experiments on fronts, Part I: Density-driven boundary currents. *J. Geophys. Astrophys. Fluid Dyn.*, *19*, 159–187, 1982.

Johannessen, O. M., Note on some vertical current profiles below ice floes in the Gulf of St. Lawrence and near the North Pole, *J. Geophys. Res.*, *75*(15), 2857–2863, 1970.

Johannessen, O. M., D. Good, and C. Smallenburger, Observation of an oceanic front in the Ionian Sea during early winter 1970, *J. Geophys. Res.*, *82*(9), 1381–1391, 1977.

Kowalik, Z. and N. Untersteiner, A study of the M2 tide in the Arctic Ocean, *Dtsch. Hydrogr. Z.*, *31*, 216–229, 1978.

Leavitt, E., Surface based air stress measurements made during AIDJEX, in *Sea Ice Processes and Models*, edited by R. S. Pritchard, pp. 419–429, University of Washington Press, Seattle, Wash., 1980.

Macklin, S. A., The wind drag coefficient over first-year sea ice in the Bering Sea, *J. Geophys. Res.*, this issue.

Martin, S., P. Kauffman, and C. Parkinson, The movement and decay of ice edge bands in the winter Bering Sea, *J. Geophys. Res.*, this issue.

McPhee, M. G., An analysis of pack ice drift in summer, in *Sea Ice Processes and Models*, edited by R. S. Pritchard, pp. 62–75, University of Washington Press, Seattle, Wash., 1980.

McWilliams, J. C., and G. R. Flierl, On the evolution of isolated nonlinear vortices, *J. Phys. Oceanogr.*, *9*, 1155–1182, 1979.

Morison, J., Forced internal waves in the Arctic ocean, Ph.D. dissertation, Geophys. Program, Univ. of Wash., Seattle, Wash., 1980.

Morison, J. H., and S. P. Burke, Oceanographic buoys at Fram III and in the marginal ice zone east of Greenland (abstract), *Eos Trans. AGU*, *62*(45), 889, 1981.

Niebauer, H. J., Wind and melt driven circulation in a marginal sea ice edge frontal system: A numerical model, *Cont. Shelf Res.*, *1*(1), 29–78, 1982.

Data from the drifting buoys were also examined to see if they reveal any eddy motion. The wind-driven ice motion was subtracted by using the method of *Thorndike and Colony* [1982]. The results indicated that the two ice edge buoys (1566 and 1568), separated by 30 km, both took part in a cyclonic motion, with a period of 8-10 days and a scale of 10-20 km, resulting in an orbital velocity of the order of 0.10 m/s.

Finally, examination of the CTD data reveals a number of features which give the appearance of eddies. For example, examination of Figure 17 shows two distinct upward displacements of the pycnocline at stations 219 and 216, superimposed on the overall upwelling pattern. The height of the displacements, relative to the average upwelling shape, is about 7 m. The horizontal scale of these features is about 15 km. Traces of them in density contours extend to 200 m, but the geostrophic velocity contours display nearly no motion below the pycnocline. Apparently, the features are confined to the mixed layer.

The velocity displays a cellular pattern. The cell at the ice edge shows a maximum speed of 0.20 m/s down-ice while the other cells show a speed of about 0.05 m/s with directions alternating between up-ice and down-ice.

On the basis of the facts cited above, the vertical displacement pattern may be interpreted as a manifestation of cyclonic eddies with a dimension of 15 km and orbital velocities of 0.05 to 0.10 m/s. The horizontal scale of the features agrees with the scale of the eddies seen in the SAR image as well as the Rossby radius of deformation, $L = 3$ km. Because of the CTD station spacing of 5 km, the displacements are not fully resolved, suggesting that aliasing, by internal waves for example, could be a problem. However, a sequence of yo-yo CTD measurements near the ice edge indicated that the internal wave rms amplitude was about 1 m, well below the eddy signals.

The propagation speed of the eddies is limited by the maximum phase speed of Rossby waves, expressed by *McWilliams and Flierl* [1979] as

$$C = \beta L^2 \tag{4}$$

where β is the variation in the Coriolis parameter with latitude. This speed is about 0.9×10^{-4} m/s in the NORSEX region and is thus negligible in comparison to the mean water velocity. Consequently, the eddies most likely travel with the mean flow once they are generated.

Eddies may arise either as a result of baroclinic instabilities, which involve the release of potential energy from a stratified fluid with vertical velocity shear, or as a result of barotropic instabilities, which involve the withdrawal of kinetic energy from a mean horizontal shear. During NORSEX, horizontal and vertical shear occurred in the ice edge region.

A simple way of examining conditions required for baroclinic instability was suggested by *Phillips* [1954]. He considered a two-layer rotating flow with uniform velocities in each layer. With the existence of vertical shear and setting β equal to zero, a perturbation on the flow will grow if

$$K^2 < \frac{2f^2 L_s^2}{g'} [H(H_t - H)]^{-1.2} \tag{5}$$

where L_s is the horizontal scale of the motion, H is the mixed layer depth, H_t is the total depth, and g' is reduced gravity. The nondimensional wave number K is defined as $2\pi L_s / L^*$ where L^* is the wavelength of the perturbation [*Pedlosky*, 1979]. The growth rate of the disturbance is dependent on the magnitude of the shear. The inequality (5) is fulfilled at the NORSEX site where L_s (≈ 10 km) is the width of the zonal flow defined by the current jet and L^* is the ice edge meander wavelength, 25 to 40 km, observed in Figure 16, and therefore the upper layer current appears to be baroclinically unstable.

The necessary condition for barotropic instability is that there is an inflexion point in the horizontal profile of velocity [*Pedlosky*, 1979]. On the basis of current measurements and the existence of an ice edge jet, one can infer that this criterion is also fulfilled in the NORSEX region.

Recent work by *Griffiths and Linden* [1981, 1982] allows us to make some statement as to the relative importance of baroclinic and barotropic instabilities when both are possible. *Griffiths and Linden* [1981] studied barotropic and baroclinic instabilities in a two-layer rotating tank experiment. They were able to interpret the stability of vortices in terms of mixed barotropic and baroclinic instabilities by varying two critical parameters: θ, the square of the ratio of the internal Rossby radius of

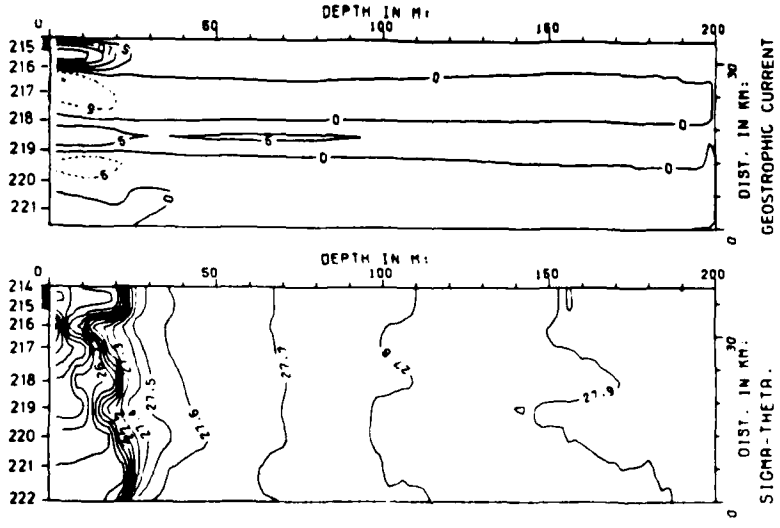

Fig. 17. Density structure and geostrophic velocities (centimeters per second) from CTD section X. Down-ice velocity (solid line). Stations indicated at the top of the sections.

NORSEX Group, The Norwegian Remote Sensing Experiment (NORSEX) in the marginal ice zone north of Svalbard, *Science*, in press, 1982.

Paquette, R. G., Cruise report USCGC Northwind, October–November 1981, Naval Postgrad. School, Monterey, Calif., February 1982.

Pease, C. H., S. A. Salo, and J. E. Overland, Drag measurements for first-year sea ice over a shallow sea, *J. Geophys. Res.*, this issue.

Pedlosky, J., *Geophysical Fluid Dynamics*, Springer-Verlag, New York, 1979.

Phillips, N. A., Energy transformations and meridional circulations associated with simple baroclinic waves in a two-level, quasi-geostrophic model, *Tellus*, *6*, 273–280, 1954.

Roberts, J., and T. D. Roberts, Use of the Butterworth low-pass filter for oceanographic data, *J. Geophys. Res.*, *83*(C11), 5510–5514, 1978.

Røed, L. P., and J. J. O'Brien, Geostrophic adjustment in highly dispersive media: An application to the marginal ice zone, *J. Geophys. Astrophys. Fluid Dyn.*, *18*, 263–278, 1981.

Røed, L. P., and J. J. O'Brien, A coupled ice-ocean model of upwelling in the marginal ice zone, *J. Geophys. Res.*, this issue.

Smith, S. D., E. G. Banke, and O. M. Johannessen, Wind stress and turbulence over ice in the Gulf of Saint Lawrence, *J. Geophys. Res.*, *75*(15), 2803–2812, 1970.

Smylie, D. E., G. K. Clarke, and T. J. Ulrych, Analysis of irregularities in the earth's rotation, *Methods Comput. Phys.*, *13*, 391–430, 1973.

Sundvor, E., G. L. Johnson, and A. M. Myhre, Some aspects of morphology and structure of the Yermak Plateau, northwest of Spitzbergen, *Sci. Rep. 8*, pp. 1–26, Seismol. Observ., Univ. of Bergen, Bergen, Norway, 1982.

Svendsen, E., K. Kloster, B. Farrelly, O. M. Johannessen, J. A. Johannessen, W. J. Campbell, P. Gloersen, D. Cavalieri, and C. Matzler, Norwegian Remote Sensing Experiment: Evaluation of the Nimbus 7 scanning multichannel microwave radiometer for sea ice research, *J. Geophys. Res.*, this issue.

Thorndike, A. S., and R. Colony, Arctic Ocean Buoy Program, Data Report, 1 January 1980–31 December 1980, Polar Sci. Center, Univ. of Wash., Seattle, Wash., 1981.

Thorndike, A. S., and R. Colony, Sea ice motion in response to geostrophic winds, *J. Geophys. Res.*, *87*(C8), 5845–5852, 1982.

Vinje, T. E., Sea ice conditions in the European sector of the marginal seas of the Arctic, 1966–1975, *Arbok Nor. Polarinst.*, *1975*, 163–174, 1977*a*.

Vinje, T. E., Sea ice studies in the Spitzbergen-Greenland area, *Landsat Rep. E77-10206*, U.S. Dep. of Commer., Natl. Tech. Inf. Serv., Springfield, Va., 1977*b*.

Wadhams, P., Sidescan sonar imagery of the sea ice in the Arctic Ocean, *Can. J. Remote Sens.*, *4*, 161–172, 1978.

Wadhams, P., The ice cover in the Greenland and Norwegian seas, *Rev. Geophys. Space Phys.*, *19*(3), 345–393, 1981.

Wadhams, P., and V. A. Squire, An ice-water vortex at the edge of the East Greenland Current, *J. Geophys. Res.*, this issue.

(Received June 16, 1982;
revised September 15, 1982;
accepted September 23, 1982.)

Appendix C

EOS, Vol. 63, No. 35, Pages 627–636, August 31, 1982

The *Fram 3* Expedition

T. O. Manley,[1] L. A. Codispoti,[2] K. L. Hunkins,[1] H. R. Jackson,[3] E. P. Jones,[4] V. Lee,[5] S. Moore,[6] J. Morison,[7] T. T. Packard,[2] and P. Wadhams[6]

Introduction

On the fourteenth of March 1981, *Fram 3*, the third in a series of four U.S. manned ice camps, was established in the eastern Arctic Ocean at 84.32°N, 20.07°E for oceanographic and geophysical research in the Eurasian Basin north of the Greenland-Spitzbergen Passage.

Investigators from several institutions in the United States, as well as from Canada and England, participated in studies of physical and chemical oceanography, low-frequency underwater acoustics, geophysics, and the mechanics and propagation of waves through sea ice. A Bell 204 helicopter and crew were stationed at *Fram 3* throughout the drift in order to support research efforts and camp operations. Several oceanographic buoys that used satellite telemetry were deployed during this time period.

Oceanographically, the *Fram 3* region is of interest because of the proximity of the polar front, which separates the outflowing Arctic surface water from the inflowing Atlantic water in the Greenland-Spitzbergen Passage and northward. Significant amounts of heat and salt are transferred through this strait as compared to other passages into the Arctic Ocean, such as the Bering Strait and the Arctic Archipelago [*Aagaard and Greisman*, 1975]. Variations in these transports of heat and salt through the Fram Strait may prove to be a significant factor in climate change. Estimates of vertical fluxes in heat and salt were also part of the ongoing experiments of the *Fram* expeditions. These would help determine spatial variations of heat loss from the Atlantic water into the upper layers of the Arctic Ocean (less than 200 m). It was also hoped that data might also provide more insight into the origin and effects of the steep pycnocline that lies directly beneath the mixed layer (50 m) and the upper extent of the Atlantic water (200–500 m). Current theory suggests that this layer is the product of wintertime ice formation on the shelves surrounding the Arctic Ocean. The resultant cold, saline shelf water is later advected into the Arctic Ocean on surfaces of constant density that reside in the depth range of 50 to 200 m. Due to the very large gradients of temperature and salinity in this depth range, the vertical transfer of heat from the Atlantic water to the upper layers of the Arctic Ocean is effectively minimized. Mesoscale CTD (conductivity, temperature, and depth) surveys were also conducted by helicopter to depths of 500 m in order to expand the areas of observation as well as to map various features and their temporal variations on length scales of 10 to 300 km. A profiling current meter-CTD unit was also used at the main camp to study the response of the upper ocean to storms.

At camp, samples for chemical and biochemical analysis, ranging in volume from 1.2 to 100 l, were taken at many levels throughout the water column. Various projects were designed to study the concentrations of tritium, oxygen, alkalinity, nutrients, respiratory enzymes, trace metals, ammonia, dissolved silicon, and bomb-produced C-14.

Further geophysical information was also to be gathered in the areas of the Nansen Basin and Yermak Plateau. The Nansen Basin is of interest because of its thin oceanic crust, which is a result of the very slow spreading of the Arctic Mid-Ocean Ridge, located several hundred kilometers to the west. The Yermak Plateau may be continental in origin, however, it does not fit well into a reconstruction of the local continental land masses. In order to study these features, observations of heat flow, gravity, short sediment cores, seismic reflection profiles, and continuous precision depth recordings were made at *Fram 3*. Several seismic refraction lines were also conducted in the vicinity of the Yermak Plateau and within the Nansen Basin with the aid of the helicopter.

With all scientific goals accomplished, *Fram 3* was evacuated on May 13, 1981, at a position of 81°43'N and 3°15'E. The resulting net drift of 361 km proved to be much longer than that of *Fram 1* (163 km) and *Fram 2* (83 km) stations during the previous years. This not only allowed experiments to be carried out over a large geographical area but also over a range of ocean depths, from a maximum of 4088 m in the Nansen Basin to a minimum of 727 m above the Yermak Plateau. Figure 1 shows the drift tracks of the three *Fram* stations superimposed on the general bathymetry of the Arctic Ocean.

Background

After completion of the Arctic Ice Dynamics Joint Experiment (AIDJEX) in the Beau-

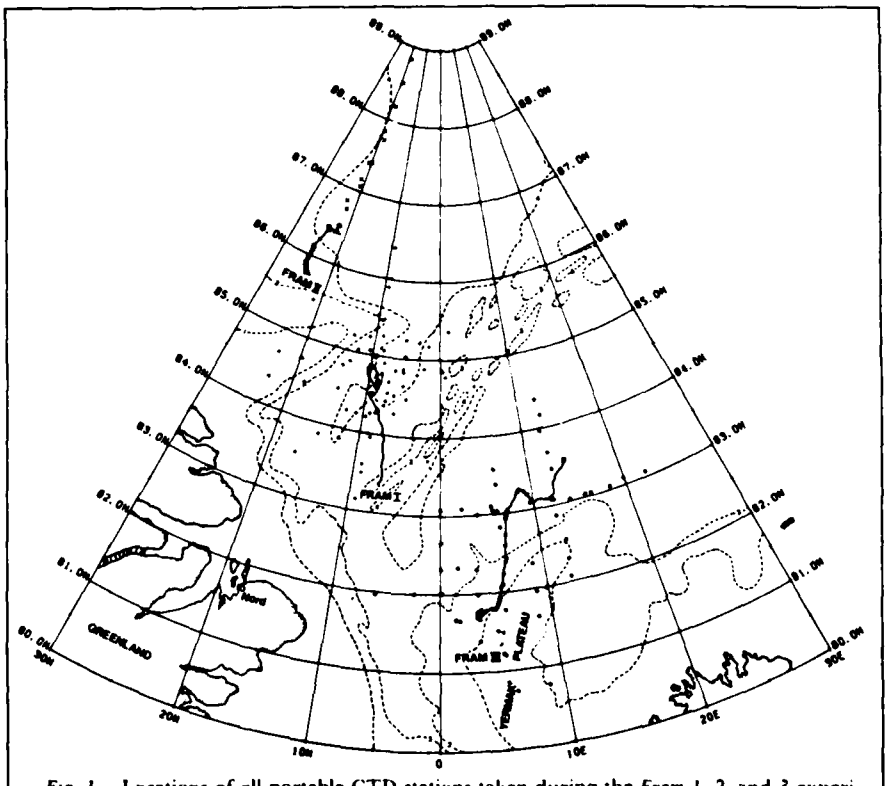

Fig. 1. Locations of all portable CTD stations taken during the *Fram 1*, *2*, and *3* experiments. Drift tracks of the individual camps are also shown in reference to Greenland, Spitzbergen, and bottom topographic contours. The end of the drift track is labeled by the camp identification. Depths are given in kilometers.

[1]Lamont-Doherty Geological Observatory of Columbia University, Palisades, New York.
[2]Bigelow Laboratory for Ocean Sciences, West Booth Bay Harbor, Maine.
[3]Atlantic Geoscience Center of Bedford Institute of Oceanography, Nova Scotia, Canada.
[4]Atlantic Oceanographic Laboratory of Bedford Institute of Oceanography, Nova Scotia, Canada.
[5]Tritium Laboratory, Rosenstiel School of Marine and Atmospheric Science, University of Miami, Miami, Florida.
[6]Scott Polar Research Institute, Cambridge, England.
[7]Polar Science Center, University of Washington, Seattle, Washington.

0096-3941/82/6335-0627$01.00

fort Sea in 1976, where ice mechanics in the central pack was emphasized, the United States made a concerted effort to begin geophysical and oceanographic investigations in the eastern Arctic Ocean. The *Fram* expedition series of short-duration manned camps located on the drifting pack ice north of Greenland has been the focus of this effort. Cooperation and participation from Norway, Denmark, and Canada in several of the expeditions have been an important aspect in these projects.

The project name *Fram* echoes that of the specially designed ship that was frozen into the pack ice of the Arctic Ocean near the New Siberian Islands by the Norwegian explorer Fridtjof Nansen, in a milestone of polar scientific exploration. During the drift of the original *Fram* (1893–96), an unprecedented amount of information was collected over the deep ocean of the Eurasian Basin.

The first of the modern *Fram* camps was established on the drifting ice at a position of 84°24'N, 6°00'W, on March 11, 1979 (Figure 1). *Fram 1* was a U.S. drifting ice station that had scientific and logistic participation by Norway, Denmark, and Canada. Away from the main camp a CTD survey, seismic refraction lines, microearthquake investigation, and polar bear migration studies were supported by helicopter. At the main camp there were programs in physical, chemical, and biological oceanography, as well as surface weather monitoring. Although the drift of the camp did not reach its anticipated destination by evacuation time, a large amount of geophysical and oceanographic data were obtained [*Kristoffersen*, 1979; *Hunkins et al.*, 1979*a*, *b*].

Preliminary scientific results from *Fram 1* were presented at the special session "Arctic Geophysics and Oceanography: LOREX and *Fram 1*" during the American Geophysical Union Spring Meeting 1980. Interesting results suggest that the crust in the Amundsen Basin is less than 3 km thick and is related to the slow spreading rate of the Arctic Mid-Ocean Ridge. *Reid and Jackson* [1981] have also formulated a theoretical model for the relationship between crustal thickness and spreading rate for the ridge. Data not only from the *Fram* expedition but also from numerous areas around the world agree with the model. Also observed on one of the refraction lines was a local hot spot over which the crust was significantly thicker, 8 km [*Jackson et al.*, 1982].

Although baroclinic eddies of the type highly prevalent in the Beaufort Sea north of Alaska [*Manley*, 1981; *Dixit*, 1978; *Hunkins*, 1974; *Newton et al.*, 1974] were not observed, a prominent front was found in the mixed layer. Heat flux from the Atlantic water into the surface mixed layer is effectively minimized by the steep pycnocline overlaying the Atlantic water, even close to the main polar front region [*Aagaard et al.*, 1979; *McPhee*, 1980*a*]. Both portable and camp-based CTD measurements documented a type of frontal intrusion of colder, more saline water from the south and may have originated from the arctic continental shelves [*Aagaard et al.*, 1979; *Hunkins and Manley*, 1980; *McPhee*, 1980*b*].

In the following spring, *Fram 2* was established on March 14 for the study of long-range, low-frequency, underwater acoustics, and later its two manned satellites, camp 1 and camp 2, were also set up [*Allen et al.*, 1980]. Marine geophysics and physical oceanography were conducted at the main camp as well as along lines radiating away from the

James Morison *is a physical oceanographer at the Polar Science Center, University of Washington, Seattle. He holds a B.S. and an M.S. (mechanical engineering) from the University of California at Davis and received a Ph.D. in geophysics from the University of Washington in 1980. He is a member of Sigma Xi, the American Geophysical Union, and the Current Meter Technology Committee of the IEEE Council on Oceanic Engineering. His current research interests are in experimental and theoretical studies of the dynamics and thermodynamics of the upper Arctic Ocean and marginal ice zones.*

Peter Wadhams *is assistant director of research at the Scott Polar Research Institute, University of Cambridge, England, and leader of the Sea Ice Group there. His research interests include the topography and thickness distribution of sea ice in the Arctic Ocean, the interaction of ocean waves with sea ice, and the dynamics of ice edge processes such as band and eddy formation. From 1980–81 he was visiting professor at the Naval Postgraduate School, Monterey, and he is involved with the planning of the MIZEX ice edge experiment.*

Stuart Moore *is a research technician at the Scott Polar Research Institute, working primarily for the Sea Ice Group. He is involved mainly in the design and development of field and laboratory equipment and has participated in numerous Arctic and Antarctic field experiments.*

Valery Lee, *B.S. (earth and planetary sciences) M.I.T., M.S. (physical oceanography) University of Miami, a newcomer to arctic research and ice camps, she says she's already hooked. Valery is working with the Tritium Lab in Miami, where they do proportional gas counting to measure tritium and radiocarbon levels in the ocean. She likes to get out in the field and do some hands-on oceanography so as not to lose touch with 'what it's all about.' Sailing her 15' knockabout in Biscayne Bay provides an excellent antidote for those ice-camp blues.*

Lou Codispoti *is a principal investigator at the Bigelow Laboratory for Ocean Sciences. He received his B.S. in chemistry from Fordham University and his M.S. and Ph.D. in oceanography from the University of Washington. He is a member of the American Geophysical Union, the American Society of Limnology and Oceanography, and the Arctic Institute of North America. His research interests include nutrient and carbon dioxide chemistry in highly productive regions, the nitrogen cycle in oxygen deficient waters, and the chemical oceanography of the Arctic Ocean.*

H. Ruth Jackson *received a B.Sc. from Dalhousie University and an M.Sc. in geophysics from Durham University in 1978. She is employed by the Atlantic Geoscience Centre of Bedford Institute of Oceanography. She participated in the Fram 1, 2 and 3 expeditions and is involved in continuing research in the arctic.*

Ted Packard *is a principal investigator at the Bigelow Laboratory for Ocean Sciences. He received his B.S. in life sciences from M.I.T. and his M.S. and Ph.D. in oceanography from the University of Washington. His research is focused on biologically regulated chemical reactions in the ocean. He is a member of the American Chemical Society, the American Geophysical Union, the American Society of Limnology and Oceanography, and the Catalan Bio[illegible]*

Kenneth H[illegible] [illegible] *gravity and [illegible] the large-scale [illegible] eddies [illegible] He is al[illegible] canyon[illegible] oceanograph[illegible] York*

[illegible] *physical oceanography. His dissertation [illegible] mesoscale eddies of the Arctic Ocean and their characteristics and effects on energy [illegible] balances. Research interests include [illegible] physical oceanography in the Arctic Ocean.*

Peter Jones *obtained his education at the University of British Columbia, receiving a Ph.D. in 1963. Since 1973 he has been at the Bedford Institute of Oceanography, where much of his work has focused on the chemical oceanography of arctic regions.*

station, using a Bell 204 helicopter as in the *Fram 1* experiment. Scientific objectives and preliminary results of the underwater acoustic program are given by *Dyer and Baggeroer* [1980] and *Baggeroer and Dyer* [1982]. Some of the more notable results were the highly variable ambient noise conditions and good signal-to-noise ratios from backscattering of signals by features as far away as the Chukchi Sea. Seismic refraction work at *Fram 2* indicates that 2 to 3 km of sediment overlay a crust of less than 5 km, agreeing fairly closely with the *Fram 1* results [*Duckworth et al.*, 1982].

A subsurface mesoscale eddy was observed on a helicopter traverse to camp 1 from *Fram 2*. This is only the second observation of a subsurface mesoscale eddy in the Eurasian Basin. The first observation of such a feature was made by Shirshov in 1937 from the Soviet drifting ice station *NP-1* [as reported by *Belyakov*, 1972]. Thickness of the eddy was about 175 m and was in the depth range of 50 to 225 m. The depth of maximum angular velocity was calculated to be at 90 m. These characteristics are similar to those observed in the Beaufort Sea during the main AIDJEX experiment.

Staging of *Fram 3*

In late February of 1981 the advance team for *Fram 3* accompanied a group of U.S. Army parachute riggers from the 612th QM Company of Fort Bragg, North Carolina, as well as the support crew and officers of three U.S. Air Force C-130 Hercules transports from the 317th Tactical Air Wing of Pope Air Force Base, North Carolina, to Thule, Greenland. These C-130's were then used to transport all scientific and logistic gear to the Danish base at Nord on the northeast corner of Greenland, while the Army riggers at Thule prepared the necessary lumber, fuel, and explosives for eventual C-130 paradrops over *Fram 3*.

A DeHavilland Twin Otter and a specially modified DC-3 'Tri-Turbo' were then used for location, establishment, and support of the drifting ice camp. On March 13, *Fram 3* was established on a large multiyear floe that measured 3 km by 5 km and had an average thickness of 4 m. Bad weather and radio communications prevented further flights to *Fram 3* until 5 days later.

By mid-April, 203,000 pounds of fuel, lumber, and explosives were paradropped to *Fram 3* by the C-130's. An additional 75,000 pounds of scientific and logistic gear were landed at *Fram 3* by way of 24 Twin Otter and five 'Tri-Turbo' flights. From April 6 to May 5 (last day of the scientific program) an average of 19 people were stationed at the camp. By the end of the manned drift, a total of 895 'man days' had been logged at the camp.

Final evacuation from *Fram 3* was on May 13, at a position of 81°43'N, 3°15'E, 61 days after the first landing. The net drift of the ice station was 361 km to the southwest at an average drift rate of 5.9 km/d. Due to the meandering of the camp along the drift track, the total distance covered was 505 km, with a computed average drift velocity of 8.3 km/d.

Following a few days of packing at Nord, two C-130s from the 36th TAS of McChord Air Force Base, Washington, removed all remaining gear and personnel from Nord to Thule Air Force Base and then back to the United States.

Fram 3 Scientific Programs and Preliminary Results

The institutions involved in scientific programs on *Fram 3* and available preliminary results are listed below.

Lamont-Doherty Geological Observatory

Station physical oceanography. Profiles of conductivity, temperature, and oxygen were made to depths of 1000 m at least three times each day, using a Neil Brown CTD equipped with an oxygen sensor. Stations to the bottom of the ocean were taken on a weekly basis. A pinger mounted on the CTD permitted data to be taken within a few meters of the bottom. A 12-bottle rosette sampler and reversing thermometers were used to obtain temperature, salinity, and pressure data for later calibration.

Additional CTD stations were taken to provide geochemists with small 1.2-l samples of water for the study of tritium, oxygen, dissolved nutrients, and gases within the water column; to provide intercalibration stations between the portable ODE (ocean data equipment) and Neil Brown CTD's; and to provide a concurrent station at *Fram 3* at those times that the portable CTD was away from camp on a helicopter transect.

Preliminary results show passage of the main camp through the polar front, a somewhat linear surface feature on the order of 100 km wide and extending to a depth of roughly 300 m. Large temperature and salinity variations were observed frequently within this depth range. Fine structure was also highly variable in this area. Yo-yo CTD stations that were taken every 20 min to depths of 400 m were, in several cases, inadequate for keeping track of the individual fine-structured features. Well-mixed boundary layers were also observed at abyssal depths as well as along the slope and top of the Yermak Plateau.

Mesoscale helicopter oceanographic survey. Helicopter mobility provided the means to study mesoscale features and their spatial variability in the upper 500 m. This was accomplished by using a portable CTD, as in the *Fram 1* and *Fram 2* expeditions. Figure 1 shows the positions of the CTD stations taken in the vicinity of each of the *Fram* ice camps. A major objective of this program was to map the polar front in the vicinity of the *Fram 3* drift track. Another objective was to study any eddies within the region. It is hoped that further knowledge about these features will aid in the understanding of lateral mixing within the Arctic Ocean and of transport processes across the polar front. The camp passed over two features, 15 and 25 km across, of anomalously high salinity and temperature, which had apparently originated from Atlantic water. They appear to be eddies shed by the polar front. Work done by *Hunkins* [1981] indicates that this region is baroclinically unstable and that features with a scale of approximately 30 km are the fastest growing (doubling time of 2 weeks).

Alignment of the polar front was generally NE-SW. Its location, on the basis of salinity, was fairly stationary over the 1-month observation period, although temperatures showed a more variable pattern.

Ocean currents. The properties of inertial and internal waves were investigated with an array of five Aanderaa current meters equipped with conductivity, temperature, and pressure sensors. Two strings of current meters were deployed—one in a lead at the edge of the large *Fram* ice floe, 5 km from the camp; and one at camp itself. The 'lead string' had instruments suspended at depths of 25 and 100 m, while the 'camp string' had instruments at 25, 100, and 480 m.

The 100-m lead instrument documented the passage of the camp through part of the frontal zone. Superimposed upon the frontal transition of temperature and salinity along the steady southwest movement of the camp are the signatures of the anomalous intrusion of warmer, more saline water (Figure 2), previously described in the mesoscale helicopter oceanographic survey. Data from two Aanderaa current meters (25-m lead, 480-m camp) were discarded because of flooding and circuitry problems.

Hydroacoustic observations. Studies of underwater sound propagation were conducted by using sensitive hydrophones and a single

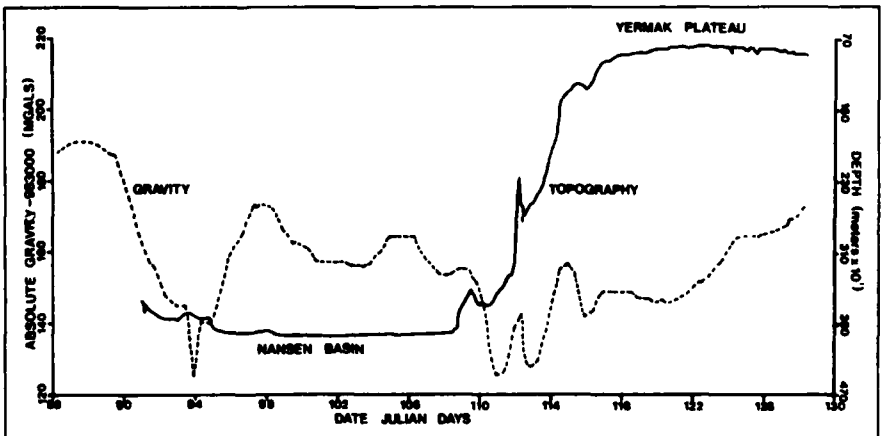

Fig. 2. Temperature and salinity time series recorded at the edge of the large *Fram 3* ice floe. Data were taken by an Aanderra current meter suspended at a depth of 100 m.

geophone. Hydrophones were placed at 1 km and 3 km away from the camp and at depths of 46 m and 60 m, respectively. The geophone was placed on the surface of the ice at a distance of 1.5 km away from the camp. Data were continuously recorded on Hewlett-Packard FM recorders.

Single earthquakes, as well as earthquake swarms, were recorded frequently, with one earthquake recorded every day on the average. Although epicenters of the earthquakes could not be fixed because of the single recording site, most of them apparently originated from the Arctic Mid-Ocean Ridge.

Geophysical observations. A marine geophysical program provided background data on position, depth, magnetic declination, floe azimuth, and gravity. A geophysical data report summarizes these results [*Hunkins et al.*, 1981]. Figure 3 shows the depth and gravity field along the drift track of *Fram 3*.

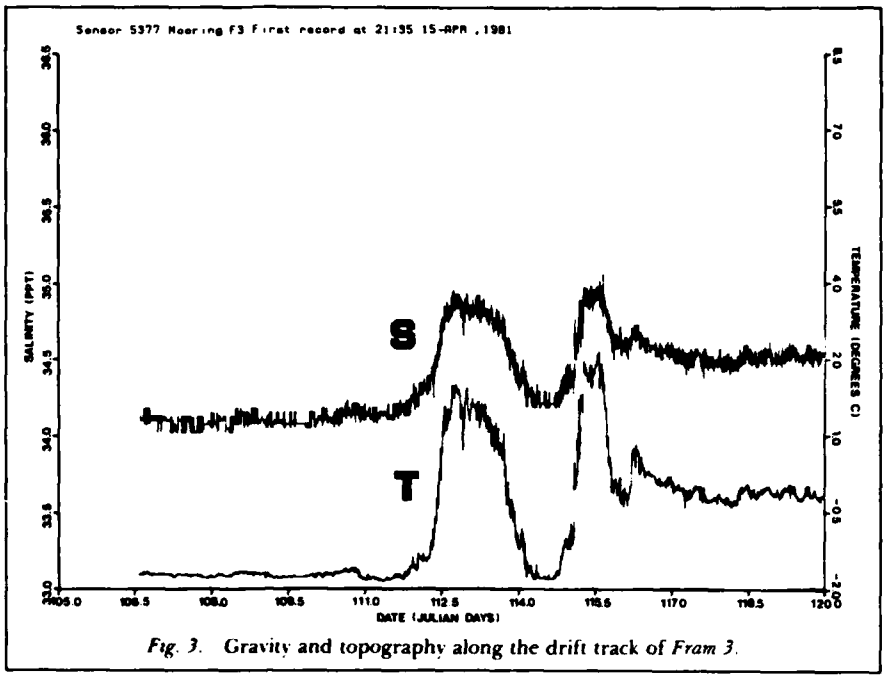

Fig. 3. Gravity and topography along the drift track of *Fram 3*.

Bedford Institute of Oceanography

Chemical oceanography. The Bedford Institute of Oceanography's primary program for chemical oceanography included measurements of oxygen, salinity, alkalinity, nutrients (nitrate, phosphate, silicate), trace metals (Mn, Fe, Ni, Cu, Zn, Cd), and radionuclides (Cs-137, Sr-90). The goal in measuring the first group of components, oxygen, salinity, alkalinity, and nutrients, was to characterize the water in the Eurasian Basin and above the Yermak Plateau and to study chemical processes, e.g., nutrient regeneration, that occur in the Arctic Ocean. More than 100 samples were collected at fairly closely spaced depth intervals from 3800 m to the surface, as the ice camp drifted toward and over the Yermak Plateau. For radionuclides and trace metals the goal was to characterize the water column and to see if there were any near-surface higher concentrations associated with Bering Sea water, as has been observed near the North Pole on the 1979 LOREX expedition [*Weber*, 1979]. Because sample collection was more difficult, especially for the radionuclides that required 100 l of water, fewer samples were collected. About 20 samples for trace metals and 15 for radionuclides were collected between depths of 2500 m and the surface.

A secondary program was to collect ice samples for analysis of alkalinity and some major ions (Ca, Mg, Cl, and SO_4). The goal of this program was to analyze the ice to detect chemical differentiation of ions, which occurs during freezing, and hence possibly to be able to predict ice meltwater content in near-surface seawater from an analysis of major ion content. Altogether, about 15 different ice samples were collected from leads, pressure ridges, and one ice core.

Analyses of the samples are presently underway, and most should be complete within about 3 months. Detailed interpretation of the results will take longer and will be done in conjunction with the physical oceanographic measurements.

Seismics and heat flow. The Atlantic Geoscience Centre of Bedford Institute of Oceanography ran a geophysical and geologic sampling program on *Fram 3* that consisted of seismic refraction, seismic reflection, heat flow, and coring.

The seismic refraction program involved the use of a tethered ocean bottom seismometer. The sound source was from 20- to 100-kg TNT charges carried away from the receiver by helicopter and detonated in areas where thin ice made access to the water possible. A 150-km line along anomaly 7 (26 m.y.) in the Nansen Basin was completed in an area where oceanic crust formed by slow spreading could be investigated. Three lines were run on the Yermak Plateau. Line 2 was run in water depths of about 2000 m on the slope of the Yermak Plateau. Line 3 was parallel to line 2 but on the top of the plateau, and line 4, also on the plateau, was run perpendicular to line 3.

The reflection profiling system was in operation at *Fram 3* from April 11 to May 5, 1981. The ocean bottom seismometer (OBS) was deployed at camp, but the refraction profiles generally ran parallel to structure and were shot away from the seismic reflection line at large angles. The reflection records provided information on the thickness of sediment below the OBS and a cross section across a portion of the Nansen Basin and the Yermak Plateau. The 9000-J Edgerton sparker provided a clear record of sedimentary layers with varying dips on the plateau, but only a minimum thickness of sediment in the basin because oceanic basement is not obviously recorded.

Along the reflection profile, 10 heat flow measurements were recorded with a 2.5-m Applied Microsystems probe, and 10 accompanying short gravity cores of about 30 cm were taken. The heat flow measurement and cores were done at water depths from 3675 to 795 m, accomplishing a line from the edge of the Nansen Basin to the top of the Yermak Plateau.

Refraction lines in the vicinity of the Yermak Plateau indicate that its northern tip is predominantly of oceanic origin, whereas the broader, more southern segment is of continental origin.

Bigelow Laboratory

Chemical and biochemical oceanography. During the first half of the *Fram 3* experiment, observations of the chemical and biochemical properties of the water column were made. These included on-site analyses for dissolved oxygen, ammonia, dissolved silicon, nitrate, nitrite, and reactive phosphorus from samples collected directly beneath the ice cover to a depth of 4000 m. On-site determinations of the activity of the respiratory electron transport system (ETS) were also made on eight samples taken from depths as great as 2000 m. Preserved samples were returned to the Bigelow Laboratory for examinations with a scanning electron microscope and for determination of their nutrient, chlorophyll, phaeophytin, particulate nitrogen, and particulate carbon contents.

With the exception of the scanning electron microscope examinations, all of the laboratory work has been completed. Initial analysis indicates that metabolic rates in the *Fram 3* water column are extremely low. Nitrite and ammonia concentrations were zero or very close to zero throughout the water column, and ETS activities were low in the upper 125 m and undetectable below that depth. This was the first time that ETS activity could not be detected in the deep-sea samples. While these results were not surprising, they will prove useful (when combined with data from other regions) in clarifying the relative importance of the processes that feed the 'deep metabolism' and in constructing an inorganic nitrogen budget for the Arctic Ocean. Although some weak maxima and minima were observed in the vertical dissolved silicon, reactive phosphorus, and nitrate distributions, there was no evidence for the presence of substantial amounts of the high nutrient waters that enter the Arctic via the Bering Strait. In addition, these data do not suggest a large contribution to the subsurface layers

from waters formed over the continental shelf during the ice formation season.

Tritium Laboratory, Rosenstiel School of Marine and Atmospheric Science

Chemical Oceanography. Detailed profiles of water samples were collected at three points along the drift track for later analysis of their tritium and ^{3}He content. Results from the earliest samples show highly tritiated water above the halocline, indicating that, at this early stage in the drift, *Fram 3* was situated in a region of outflow from the Arctic Basin. The tritium-salinity relationship of these samples seems to uphold the view that, below the upper mixed layer, Nansen Basin water is composed of binary mixtures of Atlantic source water and predominantly meteoric freshwater [*Ostlund*, 1982]. The derived tritium values of the freshwater source imply an approximate 10-year residence time for the freshwater component in the East Arctic Basin. *Fram 3* tritium-^{3}He ages, which provide an essentially independent estimate of residence time, corroborate this result.

A profile of large-volume water samples was obtained by using a 100-l General Oceanics Go-Flo Sampler. Carbon dioxide gas was extracted from these samples at camp for later radiocarbon analysis. Samples down to 1250 m show a definite presence of bomb-produced ^{14}C; deeper layers show what is most likely some bomb contribution. There is measurable tritium all the way down to 3500 m, indicating that there have been contributions at these depths of water that have been at the surface within the last 20 years.

Polar Science Center—University of Washington

Current velocity-CTD profiling, oceanographic buoys, meteorology. The scientific group from the Polar Science Center carried out three main experiments at *Fram 3*. First, a new Arctic Profiling System (APS) was used during the experiment to examine the response of the upper ocean to storms. An additional goal was to use this device to study the vertical and horizontal circulation patterns within leads. The new APS was built by the Applied Physics Laboratory of the University of Washington and is a more compact version of an earlier instrument described in *Morison* [1980]. The device is a wire-lowered instrument that measures continuous profiles of conductivity, temperature, and velocity. During the experiment, there were three storms for which good records were obtained. During these storms, casts were made to 300 m every half hour. One such sequence of profiles measures the development of a 35-m-thick mixed layer from an initially stratified condition and should provide an especially good basis for comparison with mixed layer theories. Conditions at *Fram 3* were highly variable, and dramatic changes in the water structure, especially temperature, were quite common. The variations are related to the location of *Fram 3* near the ice edge, and the data will be compared to those obtained during a previous cruise (NORSEX 79) in the same region made during the fall of 1979. Unfortunately, no leads opened near camp, and the goal of studying lead circulation was not achieved.

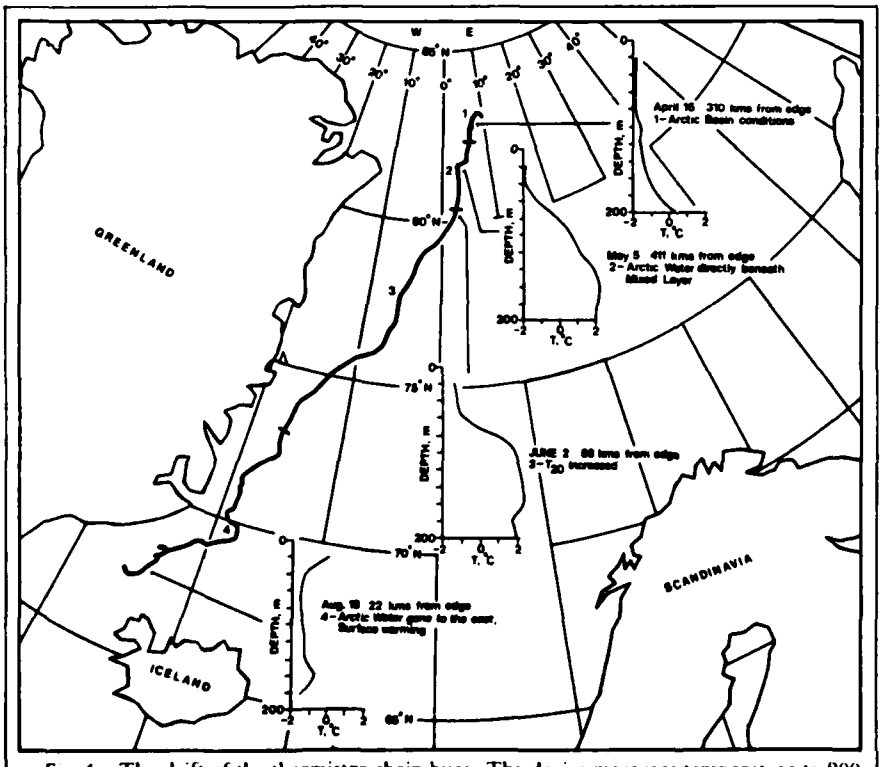

Fig. 4. The drift of the thermistor chain buoy. The device measures temperature to 200 m and transmits through the ARGOS system. During segments (2) and (3) of the drift, the buoy was over warm Atlantic water. During segments (1) and (4) it was over cold polar water.

The second experiment involved the deployment and testing of two new oceanographic buoys built by the Polar Research Laboratory. The buoys are being developed to provide a means of gathering long-term hydrographic data in the upper Arctic Ocean. One buoy is a thermistor buoy (T-buoy) and the other is a temperature-conductivity buoy (T-C buoy).

The T-buoy incorporates an electronics/ARGOS transmitter package in an aluminum tube and a Kevlar cable with thermistors imbedded in it every 20 m, hanging to a depth of 200 m. The buoy transmits temperature from all the sensors through the ARGOS satellite system four times per day.

The buoy was installed at *Fram 3* and left there after evacuation. The primary objectives were to perform intercalibrations with the APS and T-C buoy, provide a picture of the thermal structure in the East Greenland Drift, and test the survivability of the design. Data gathered simultaneously with the APS and the T-buoy generally agree.

After the end of the experiment, the T-buoy drifted south along the coast of Greenland and through Denmark Strait. Figure 4 shows the drift track of the buoy. It is noteworthy that the T-buoy remained in a fixed relation with the three other buoys left at *Fram 3* (two from the Polar Research Laboratory and one from the Norsk Polarinstituit) until just north of Denmark Strait, indicating the *Fram 3* ice floe maintained its integrity for a remarkably long time. The T-buoy ceased functioning on August 22, near the ice edge at 67°35'N 25°41'W.

The temperature profiles in Figure 4 show characteristic thermal regimes in the drift. The first shows a deep thermocline, indicating the buoy was on the cold side of the polar front. The second and third regimes show a shallow thermocline, indicating the buoy was on the warm side of the front, in spite of being 50–100 km from the ice edge. In the fourth regime the thermocline is again quite deep, but surface heating appears to be important. Fluctuations in the temperature records on the time scale of a couple of days suggest the presence of meanders or eddies near the front. The continued survival of the instrument, even in the rigorous ice edge region, bodes well for the survivability of such buoys in the pack ice.

The T-C buoy was developed as a step toward remotely measuring both temperature and conductivity for the study of the mixed layer in the Arctic. It incorporated three temperature and conductivity sensor pairs at 15 m, 30 m, and 50 m, suspended below a surface electronics package. In this buoy, temperature and conductivity are averaged over 3-hour periods. The average values are then transmitted during a once daily, 5-hour transmission window.

The buoy was operated at *Fram 3* for the purposes of testing and intercalibration with other systems, only while personnel were at the camp. The results indicate it worked well. Instantaneous conductivity values from APS and the T-C buoy generally agree within ±0.001 s/m, and the temperature values agree within less than ±0.02° C. It has been found that the deepening of the mixed layer examined with the APS could also be observed with the T-C buoy. This illustrates the usefulness of the T-C buoy, even in studies of relatively short-term processes.

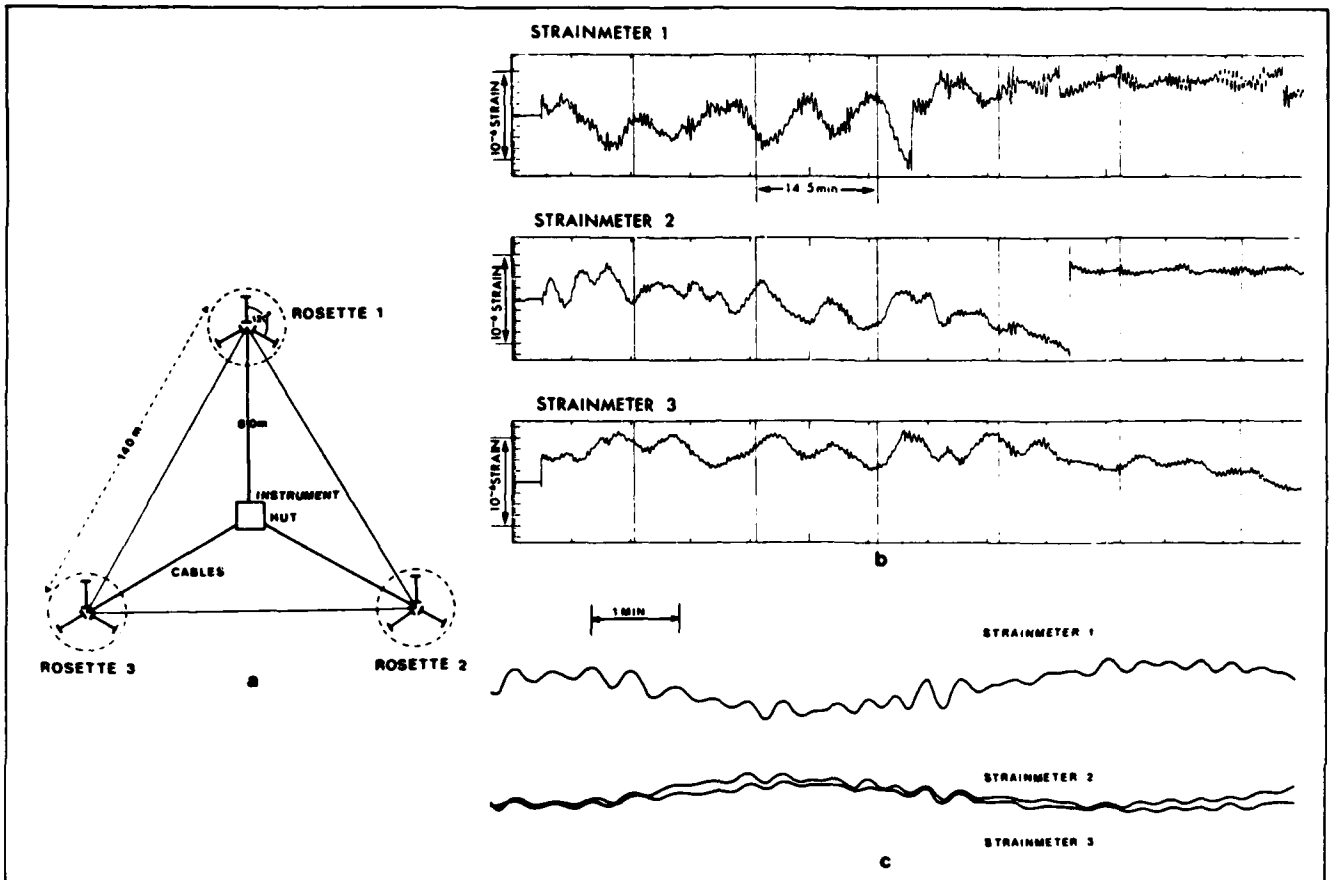

Fig. 5 (*a*) Configuration of the strain rosettes in relation to the instrument hut at *Fram 3*; (*b*) Portion of time series data obtained from one of the strain meter rosettes at *Fram 3*; (*c*) Expanded section of *b*.

Finally, a suite of atmospheric measurements were made. They included continuous recordings of temperature, atmospheric pressure, wind direction at 2 m, and wind speeds at 2 m and 10 m. The data will be correlated with changes observed with the oceanographic measurements. They will also be used in conjunction with geostrophic wind estimated from buoys, to determine geostrophic drag laws appropriate for the region.

In addition to their other projects, a thermistor chain was installed for the study of internal waves. Preliminary results suggest the presence of an active internal wave field.

Scott Polar Research Institute

Ice strain and wave propagation. The purpose of this experiment was to measure the directional energy spectrum and velocity of propagation of flexural gravity waves in the ice cover of the Arctic Ocean, using three rosettes of three strain meters, each in a triangular array, and the attenuation rate of the waves by simultaneous recording from three-strain meter rosettes, two being retained at the main camp and the third being taken to a helicopter-established camp some tens of kilometers away.

For the first experiment an existing hut at the main camp was used as an instrument hut, and three rosettes of strain meters were set up as shown in Figure 5. Each rosette consisted of three wire strain meters of high sensitivity (better than 10^{-8} strain) and rugged design evolved at SPRI for this purpose [*Moore and Wadhams*, 1980]. The strain-sensing element was a 1-m long Invar wire. Each instrument was frozen into the ice and protected by a wooden box, which was placed over it. Snow was then shoveled over each box to reduce thermal drift.

Data were recorded on digital and FM analog tapes at times when radio interference was least, i.e., at night or when there was no flying between Nord and *Fram 3*. Recording went on for 4 weeks during April–May 1981, and about 150 hours of data were recorded.

Ice thickness was measured at the strain meter sites. Other data needed for interpretation of the results and recorded by other investigators on *Fram 3* were wind speed and direction (continuously), floe rotation (daily, usually only about 1° per day), and internal wave activity (by J. Morison using thermistor chain).

During the second project, three attenuation experiments were carried out by deploying a fourth strain meter rosette away from the main camp. Positions of these remote sites relative to the main camp were 93 km north, 46 km south, and 139 km north. Each remote rosette was set up with its axes aligned as closely as possible with those at the main camp. At each remote site, at least 1 hour of data was recorded concurrently with recording at the main site.

Part *b* of Figure 5 shows a typical length of record from three strain meters in a single rosette. It is immediately apparent that there are two distinct components of oscillation present. The short-period oscillations have a typical amplitude of 10^{-7} strain and period of 30 s. An expansion of the time scale (Figure 5*c*) shows that oscillations from the three strain meters are in phase. This suggests that they are flexural gravity waves, as recorded on previous occasions in the Arctic Ocean [*Hunkins*, 1962; *LeSchack and Haubrich*, 1964]. The ice thickness at the site was 3.2 m, from which we can infer that the wave amplitude was about 3 mm. Long waves of this kind can be explained as being the envelopes of wave packets found in the open sea [*Larsen*, 1978*a*, *b*]. The Arctic Ocean ice cover, however, acts as a filter, which removes all shorter-period components by scattering or creep mechanisms. Full analysis of the results will reveal whether this is really the case, since it will give the directional spectrum of the waves (to show whether they are coming from the nearest open ocean in Fram Strait), any correlation with local wind (in case direct generation through the ice is occurring), and the attenuation rate.

The long-period oscillations apparent in Figure 5*b* were unexpected. They are of greater amplitude than the short-period oscillations—typically 5×10^{-7} strain—and have periods of about 10 min. This is far too long for any flexural gravity wave, especially since it implies a very large vertical amplitude of ice oscillation. Furthermore, on the expanded scale (Figure 5*c*), and on Figure 5*b*, it can be seen that two strain meters are in phase while the third is in antiphase. This is the result that we would expect from a wave of compression passing through the ice, i.e., a longi-

tudinal wave. Our interpretation is that (1) the ice is responding to the presence of internal waves, concurrently measured by J. Morison and found to have a typical period of 10 min or (2) the ice is responding to the very small variations in sea surface elevation associated with the internal waves.

On April 10 the long-period strain field increased greatly in amplitude some 24 hours after the onset of a 12 m/s wind. If it is true that ice acceleration generates internal waves through interaction with pressure ridge keels, then we would expect increased long-period ice strain to follow a storm. Further analysis of the joint data sets will determine whether this hypothesis is valid.

Scientific Personnel

Lamont-Doherty Geological Observatory of Columbia University. Ken Hunkins (Senior Scientist), T. O. Manley, J. Ardai, A. Gill, C. Monjo.

Bedford Institute of Oceanography. Ruth Jackson, P. Jones, D. Locke, F. Zemylak.

Bigelow Laboratory for Ocean Sciences. Lou Codispoti and Ted Packard.

University of Miami Tritium Laboratory, Florida. Valery Lee.

Polar Science Center of the University of Washington. James Morison, R. Anderson.

Scott Polar Research Institute, Cambridge, England. Stuart Moore.

Polar Research Laboratory. Sam Burke.

Support Personnel

Polar Science Center. Andy Heiberg (Operations Manager), Al Hielscher (*Fram 3* Station Manager), Imants Virsnieks (Thule Liaison).

612th QM Company, Fort Bragg, North Carolina. Lt. Pollard (Army Riggers Commander).

36th Tactical Air Support, McChord Air Force Base, Washington.

317th Tactical Air Wing, Pope Air Force Base, North Carolina. Lt. Col. M. Galey (Commander of C-130 Group).

Greenland Air Charter. Helge Siljuberg and Goren Lindmark (Bell 204 pilot and mechanic).

Bradley Air Service. Ross Michelin, Bill Smith and Gary Moore (*Fram 3* Twin Otter crew).

Polar Research Lab. Jim Aikens, Don McWilliams and Chris Hutton (Tri-Turbo crew).

Acknowledgment

This work was supported by the Office of Naval Research under contract N00014-76-C-0004 and by the National Science Foundation under grant DPP-8025744 to the Bigelow Laboratory.

References

Aagaard, K., and P. Greisman, Toward new mass and heat budgets for the Arctic Ocean, *J. Geophys. Res.*, *80*(27), 3821–3827, 1975.

Aagaard, K., E. C. Carmack, A. Foldvik, P. D. Killworth, E. L. Lewis, J. Meinke, C. A. Paulsen, The Arctic Ocean Heat Budget, *SCOR Rep. 58*, 98 pp., Geophys. Inst., Univ. Bergen, Norway, 1979.

Allen, B., J. Ardai, K. Hunkins, T. Lee, T. Manley, and W. Tiemann, Observations of position, ocean depths and gravity taken from the Fram II and Camp I drifting ice station, *CU-13-80, Tech. Rep. 13*, Lamont-Doherty Geol. Observ., Columbia Univ., Palisades, New York, 1980.

Baggeroer, A., and I. Dyer, Fram 2 in the Eastern Arctic, *Eos Trans. AGU*, *63*(14), 1982.

Belyakov, L., Triggering mechanism of deep episodic currents in the Arctic Basin (in Russian), *Probl. Arktiki Antarkt.*, *39*, 25–32, 1972.

Dixit, B., Some mesoscale flow features in the Beaufort Sea during AIDJEX 1975–1976, Doctoral dissertation, 244 pp., McGill Univ., Quebec, Canada, 1978.

Duckworth, G., A. Baggeroer, and H. Jackson, Crustal structure measurements near Fram II in the Polar Abyssal Plain, *Tectonophysics*, in press, 1982.

Dyer, I., and A. Baggeroer, Fram II in the eastern Arctic Ocean, *Eos Trans. AGU*, *61*(4), 1980.

Hunkins, K., Waves on the Arctic Ocean, *J. Geophys. Res.*, *67*(6), 2477–2489, 1962.

Hunkins, K., Subsurface eddies in the Arctic Ocean, *Deep-Sea Res.*, *21*, 1017–1034, 1974.

Hunkins, K., and T. Manley, Oceanographic measurements at the Fram I ice station (abstract), *Eos Trans. AGU*, *61*(17), 1980.

Hunkins, K., T. Manley, and W. Tiemann, Observations of position, ocean depth, ice rotation, magnetic declination and gravity taken at the Fram I drifting ice station, *CU-1-79, Tech. Rep. 1*, Lamont-Doherty Geol. Observ., Columbia Univ., Palisades, New York, 1979*a*.

Hunkins, K., Y. Kristoffersen, G. L. Johnson, and A. Heiberg, The Fram I expedition, *Eos Trans. AGU*, *60*(52), 1979*b*.

Hunkins, K., T. Manley, W. Tiemann and R. Jackson, Geophysical data from drifting ice station Fram III, *CU-3-81, Tech. Rep. 3*, Lamont-Doherty Geol. Observ., Columbia Univ., Palisades, New York, 1981.

Jackson, H., T. Reed, R. K. H. Falconer, Crustal structure near the Arctic Mid-Ocean Ridge, *Geophys. Res.*, in press, 1982.

Kristoffersen, Y., Isdriftstasjonen Fram I, Ekspedisjonsrapport, 89 pp., Norsk Polarinst., Bergen, Norway, 1979.

Larsen, L., Surface waves and low frequency noise in the deep ocean, *Geophys. Res. Lett.*, *5*(6), 499–501, 1978*a*.

Larsen, L., The effect of finite depth on the propagation of nonlinear wave packets, *J. Phys. Oceanogr.*, *8*(5), 923–925, 1978*b*.

LeSchack, L., and R. Haubrich, Observations of waves on an ice-covered ocean, *J. Geophys. Res.*, *69*(18), 3815–3821, 1964.

Manley T., Eddies of the Western Arctic Ocean—Their characteristics and importance to the energy, heat, and salt balance, Doctoral dissertation, *CU-1-80, Tech. Rep. 1*, Lamont-Doherty Geol. Observ., Columbia Univ., Palisades, New York, 1981.

McPhee, M., Oceanic heat flux in the Arctic: A peculiar thermohaline regime, *Ocean Modeling*, *31*, 1–4, 1980*a*.

McPhee, M., Heat transfer across the salinity-stabilized pycnocline of the Arctic Ocean, paper presented at IAHR Symposium on Stratified Flow, June 24–27, Trondheim, Norway, 1980*b*.

Moore, S., and P. Wadhams, Recent development in strainmeter design, paper presented at Workshop on Stress and Strain Measurement in Ice, Memorial Univ., St. John's, Newfoundland, Apr. 29–May 1, 1980.

Morison, J., Forced internal waves in the Arctic Ocean, Ph.D. thesis, Dep. Geophys., Univ. Wash., Seattle, Washington, 1980.

Newton, J., K. Aagaard, and L. K. Coachman, Baroclinic eddies in the Arctic Ocean, *Deep-Sea Res.*, *21*, 707–719, 1974.

Ostlund, H., The residence time of the freshwater component in Arctic Ocean, *J. Geophys. Res.*, *87*, 2035–2044, 1982.

Reed, I., and H. Jackson, Oceanic spreading rate and crustal thickness, *Mar. Geophys. Res.*, 5, in press, 1981.

Weber, J., The Lomonosov Ridge experiment, 'LOREX 79' *Eos Trans. AGU*, *60*(42), 1979.

Appendix D

SALARGOS TEMPERATURE-CONDUCTIVITY BUOYS

James Morison
Univ. of Washington
Polar Science Center
4057 Roosevelt Way NE
Seattle, WA 98105
U.S.A.

Samuel Burke
Polar Research Lab
123 Santa Barbara St.
Santa Barbara, CA 93101
U.S.A.

Hermann Steltner
Arctic Res. Estb.
Mitimatalik St.
Pond Inlet, NWT
Canada X0A 0S0

Roger Andersen
Univ. of Washington
Polar Science Center
4057 Roosevelt Way NE
Seattle, WA 98105
U.S.A.

Abstract

The design and testing of buoys capable of measuring temperature and salinity in ice covered oceans is described. The buoys are implanted in the sea ice and collect water temperature and conductivity data from pairs of sensors tethered to a cable suspended below the ice. The sensor data is collected and position is determined using the ARGOS satellite system.

Two tests of the buoy system are described. Comparisons of the buoy data with CTD data gathered at Fram III and with hydrocast data at Pond Inlet, NWT indicate the buoy is capable of measuring salinity with accuracies of about 0.02 o/oo for periods up to two months. Low salinity readings relative to hydrocasts at Fram III and for one sensor depth at Pond Inlet are yet to be explained. Drift due to biological fouling does not appear to be a problem.

1. Introduction

The upper Arctic Ocean is stratified by salinity because temperature fluctuations there are relatively small. Also, because salt is rejected during ice formation, buoyancy and heat flux at the surface are associated with changes in surface layer salinity rather than temperature. Therefore, in order to monitor density structure and particularly changes in the mixed layer in the Arctic Ocean, it is necessary to monitor salinity. Two SALARGOS temperature-conductivity buoys have been built and are being tested with the goal of testing the feasibility of making such measurements, unattended, over extended periods of time.

The use of moored conductivity sensors to monitor salinity is somewhat rare. The overriding concern in making such measurements has been the drift of the conductivity cells due to biological fouling. Irish (1977 and 1981) has performed several experiments using the Seabird SBE-4, electrode type, conductivity cell described by Pederson and Gregg (1979). His experiments have yielded mixed results. The first (Irish, 1977), conducted in Puget Sound in March 1974, yielded drift rates for the SBE-4 cells of 0.005 to 0.012 mmho/cm per day relative to a moored Plessey inductive cell. This unacceptably high drift rate was attributed to biological fouling. A subsequent experiment (Irish, 1981) on the New England continental shelf in early spring 1979 yielded absolute drift rates of only 0.02 o/oo in salinity over a four month period. Generally, Irish finds high drift rates where biological fouling is great and very low drifts in regions where there is little fouling (Irish, personal communication). The Arctic Ocean is a region of low biological fouling because of the low light levels (especially in winter) and cold temperatures. Thus, the prospects for moored conductivity measurements there can be viewed with some optimism.

2. Buoy Design

In as much as we wish to make long term measurements near the surface of the Arctic Ocean and cannot be assured of recovering the instrument, the SALARGOS buoy is designed to drift with the ice cover and telemeter data to land through the ARGOS satellite system. Position is also determined through ARGOS. Seabird SBE-3 temperature sensors and SBE-4 conductivity sensors were chosen for the main sensing elements because of their high accuracy and stability (better than ±0.01°C per six months for temperature and ±0.01 mmho/cm per month for conductivity is specified by the manufacturer), low power requirements, and convenient frequency output. The buoys have been designed and built at the Polar Research Laboratory (PRL) in Santa Barbara, California.

Figure 1 shows the first SALARGOS buoy in cross-section as it would appear installed in pack ice. It consists of a 0.2 m diameter aluminum tube 4.7 m long. The tube contains the data acquisition and transmission electronics and enough alkaline batteries to power the buoy for one year. The tube is inserted in a hole in the ice and floats with the antenna about one meter above sea level. A multiconductor, kevlar cable is suspended below the tube. In the first version of the buoy, shown here, three conductivity-temperature sensor pairs are attached to the cable at 15 m, 30 m, and 50 m. In a more recent version six pairs at 15 m, 30 m, 50 m, 60 m, 70 m, and 100 m are used. A pressure sensor, designed and built by PRL, is at the bottom of the sensor string. The whole buoy assembly weighs about 100 kg.

Figure 2 is a photograph of a temperature and conductivity sensor pair. A polypropylene mounting fixture is bonded to the kevlar cable and the sensors are secured to the fixture with tape. Light

Reprinted from OCEANS, September 1982

0197-7385/82/0000-1255 $00.75 © 1982 IEEE

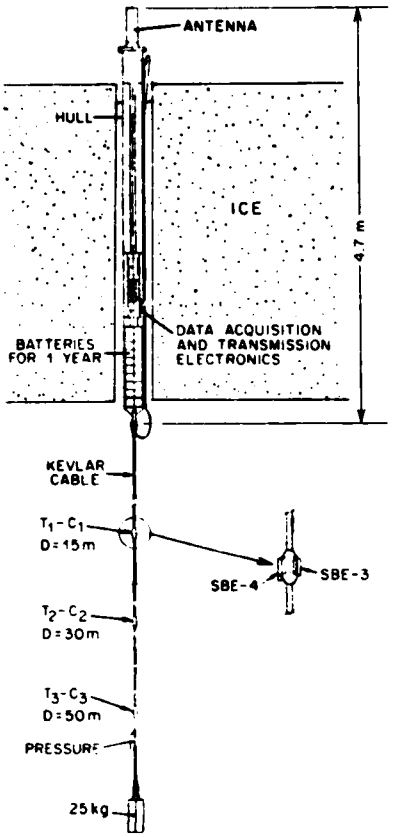

Figure 1. The SALARGOS temperature-conductivity buoy as it would appear in cross section implanted in sea ice.

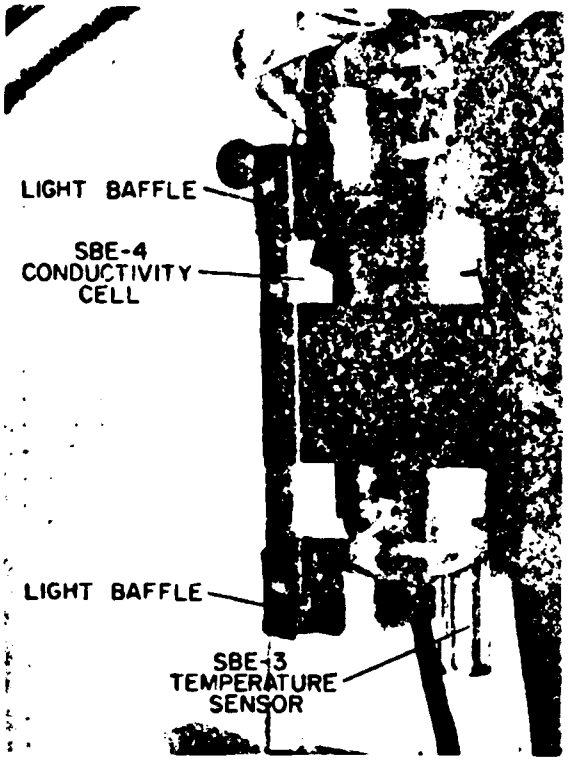

Figure 2. A temperature-conductivity sensor pair as attached to the kevlar cable of the SALARGOS buoy. Also shown are light baffles added to the conductivity cell to reduce biological fouling.

baffles, constructed of aluminum and coated with antifouling compound, have been attached to the ends of the shroud surrounding the glass conductivity cell. These baffles are meant to keep light from shining on the cells, with the aim of reducing fouling. The baffles are installed with their openings directed horizontal and opposite to each other, with the idea of enhancing the flushing of the cell.

The SALARGOS electronics are designed to sample the sensors every 12 minutes and average the samples over three hour periods. Averages covering the previous 24 hour period are transmitted through ARGOS during a five hour transmission window once per day. The electronics consist of six separate modules, the central processor unit (CPU), period counter, the input-output module, the transmitter, the 50 MHz oscillator, and the power conditioner. The basic system block diagram is shown in Figure 3. The sensors tethered below the ice are powered up and sampled under control of the CPU, which executes the 800 byte controller program held in a read only memory. Each sensor outputs a low level AC signal, the frequency of which is proportional to conductivity, temperature, or pressure. Under control of the CPU, a sensor signal is switched into an 8 bit down counter which is pre-set by the CPU to yield the sensor range and resolution required. The sensor signal initiates a gate and proceeds to decrement the down counter until the end point is reached, at which time the gate is closed. While the gate is open, a precision, high frequency clock signal is allowed to advance a 16 bit counter from a reset condition. When the gate closes, the processor reads the 16 bit counter, 8 bits at a time, and places the data in random access memory for further processing. The other sensors are sampled sequentially in the same manner.

A sensor sample sequence takes approximately 11 seconds. At the end of the sample the CPU is placed in a low powered, dormant state (idle) awaiting reactivation (interrupt) by a logic signal from an external 60 second timer. Following an interrupt condition, the CPU executes a clock routine which determines sampling times (every 12 minutes), averaging period, and ARGOS transmission times. During the three hour averaging period (16 samples taken), the 16 bit samples are continuously accumulated in a 24 bit accumulator, and are finally divided by 16 to produce an average which is stored in the 24 hour ARGOS data buffer. This data represents the time required for a specified number of sensor cycles to occur and can thus be used to compute sensor output frequency.

to compare with the LDGO data, salinities were interpolated in both time and depth from the 3 hour averages. In this sense, comparison with the LDGO data involves all three buoy sensor pairs. The Seabird conductivity sensor calibrations were determined, and the field data were analyzed, using the Practical Salinity Scale '78 (Lewis, 1980). Salinities in the upper 50 m ranged from about 33.0 o/oo at the beginning of the experiment to 34.1 o/oo at the end.

On the average the buoy salinities are 0.05 o/oo lower than the sample bottle salinities, with a slight decrease in the offset (-5.44×10^{-4} o/oo per day) with time. There is more variability in the offset at the beginning of the record. Because the change in offset implies an increase in buoy measured salinity (or conductivity), it does not appear to be due to fouling of the sensors. Fouling would lower the measured conductivity with time.

Figure 5 shows the difference between salinities measured with the buoy sensors and with the APS profiling instrument ($S_{APS} - S_{Buoy}$) during periods when mixed layer salinities were relatively constant. The conductivity and temperature sensors

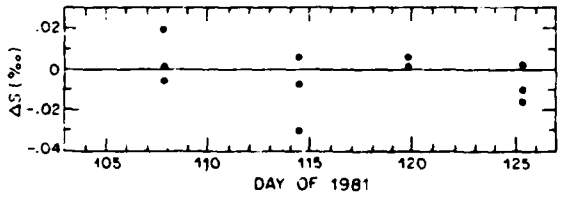

Figure 5. The difference, ΔS, between APS salinities and SALARGOS buoy salinities at Fram III plotted versus day of 1981. $\Delta S = S_{APS} - S_{Buoy}$. The values shown were computed for periods when salinities were fairly constant. The buoy salinities average 0.003 o/oo greater than the APS salinities.

used on the APS are also Seabird units and they were also calibrated at NRCC. The differences in salinity are much smaller than those shown in Figure 4. They have a mean of -0.003 o/oo and a standard deviation of 0.013 o/oo. These differences are very low, especially considering there must have been some natural variation in water properties over the 40 m separating the two instruments. The differences are less than the resolution in salinity (0.017 o/oo) determined by the resolution in temperature and the formulas relating conductivity and temperature to salinity. The small differences shown in the APS-Buoy comparison suggest that the offsets of Figure 4 are not associated with the buoy electronics or the use of the sensors in a moored configuration. They must be due to a generic error in the calibration of the sensors or some common error in the bottle measurements. These possibilities will be discussed further in light of results from the second buoy test.

Figure 6 shows salinity data gathered with the SALARGOS buoy during a short storm. The data

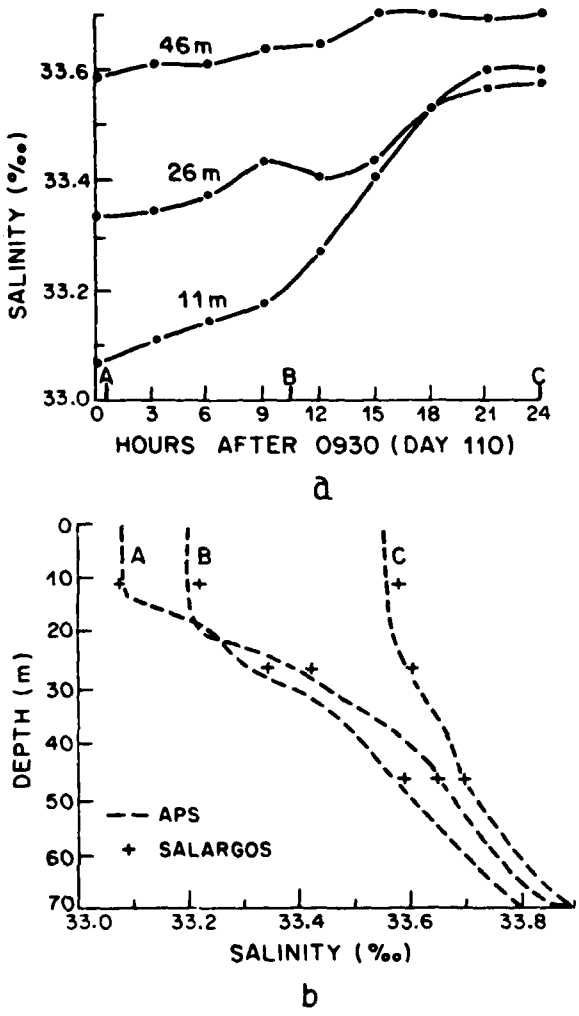

Figure 6. a) SALARGOS buoy salinity data gathered during a small storm at Fram III plotted versus time. A decrease in stratification and increase in average salinity occurs in the mixed layer.

b) APS salinity profiles and SALARGOS buoy salinities as measured at the three times A, B, and C shown in Figure 6a.

illustrate the kind of phenomena we hope to resolve with the buoy and give some idea of the magnitude of the natural variations we can expect to find. Three salinity profiles made with the APS are also shown. The mixed layer was initially stratified. During the storm the stratification decreased and the average of salinity at the three sensor depths increased 0.3 o/oo. This suggests that mixing due to surface stress occurred and that the ice was advected into a region of higher salinity. The average difference between the APS salinities and buoy salinities during this active period is -0.021 o/oo and the standard deviation is 0.017 o/oo; still a relatively small error consid-

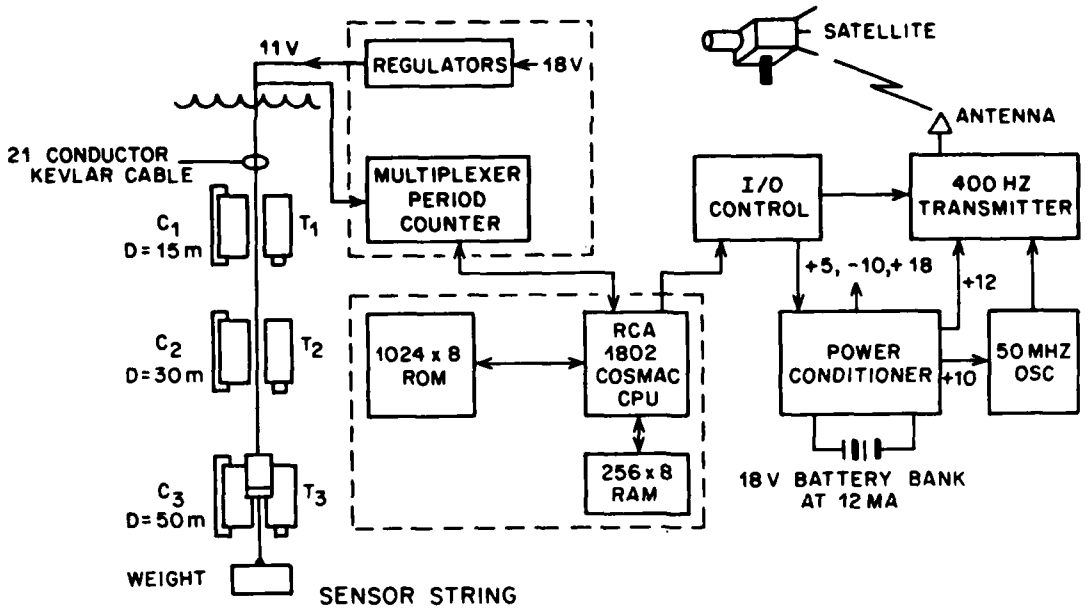

Figure 3. The basic electronics system block diagram for the SALARGOS buoy.

Once per day the CPU clock routine enables ARGOS transmissions once per minute for a five hour period. One three hour average for all sensors is sent during each transmission. During every satellite pass, 9 to 12 transmissions are received. In polar regions, about 6 satellite passes (2 satellites) are made during the five hour window and, therefore, each average is transmitted up to eight times, providing more than adequate redundancy.

The conductivity sensor data are transmitted with 16 bit resolution. When sensor frequencies and conductivities are calculated, a resolution of 10^{-4} mmho/cm results for the range of variables encountered in this application. Temperature and depth sensor data are transmitted with 8 bit resolution resulting in 0.015°C and 0.2 m resolution respectively.

3. Field Tests

There have been two field tests of the first SALARGOS buoy. In April and May 1981 the buoy was operated at the Fram III ice camp at 83°N 10°E. The second test was begun at Pond Inlet, Northwest Territories at 72.8°N 78.2°W in February 1982 and is continuing. The second SALARGOS buoy was used at the Fram IV ice station in April and May 1982 as part of an internal wave study, but data from that experiment has not been analyzed as yet.

Prior to the Fram III experiment the buoy sensors were calibrated at the Northwest Regional Calibration Center (NRCC). During the experiment the buoy was not installed in the ice but, rather, was left in a heated building. The sensor string was lowered through a hydrohole in the floor of the building. The sensor depths were 11 m, 26 m, and 46 m. The buoy was operated from day 104 (April 4) to day 126 (May 6) of 1981. During that time, a profiling current meter-CTD system, the Arctic Profiling System (APS), was also operated by our group from the University of Washington (UW), and Nansen bottle samples were taken at a depth of 26 m. Water samples were also taken as part of CTD measurements made by a group from the Lamont-Doherty *Geological Observatory* (LDGO). The water samples and APS measurements provide a basis for evaluating the buoy data.

Figure 4 is a plot of the difference ($S_{Bottle} - S_{Buoy}$) between sample bottle salinities, from the UW and LDGO hydrocasts, and the salinities measured with the SALARGOS buoy. The salinities of the UW

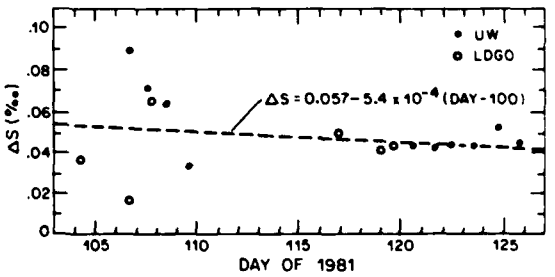

Figure 4. The difference, ΔS, between sample bottle salinities and SALARGOS buoy salinities at Fram III plotted versus day of 1981. $\Delta S = S_{Bottle} - S_{Buoy}$. A least squares linear fit to the data is shown as a dashed line. The buoy salinities average 0.05 o/oo less than the bottle salinities.

samples are compared to values interpolated in time from the 3 hour average buoy data at 26 m. In order

ering 3 hour averages are being compared to instantaneous values.

In comparing 3 hour average temperature measurements made with the buoy to those made with reversing thermometers during the UW hydrocasts, the differences, $T_{Hydrocast} - T_{Buoy}$, are found to have a mean of -0.019°C and a standard deviation of 0.010°C. Comparing the buoy temperature measurements with the four APS profiles made during calm conditions, the differences, $T_{APS} - T_{Buoy}$, average -0.004°C, and have a standard deviation of 0.006°C. These errors are on the order of the SALARGO buoy temperature resolution.

The SALARGO buoy was deployed for the second time on Day 57 of 1982 in the middle of Pond Inlet between Bylot Island and Baffin Island. The instrument was installed in the ice using the arrangement shown in Figures 1 and 2. The only difference was sensor pairs 2 and 3 were both placed at 30 m to facilitate intercomparison of the sensor data. All sensors were calibrated at NPGS just prior to the experiment. The same conductivity sensor was used for sensor pair 2 as was used at Fram III. Otherwise, different SBE-3 and SBE-4 sensors were used. The change in calibration over one year for conductivity sensor 2 was less than 0.005 mmho/cm for the range of conductivities encountered. Immediately after deployment the conductivity sensors yielded very low values, presumably because they were clogged with frazil ice which accumulated in the hydrohole during deployment. By day 57 all the sensors had come to equilibrium. The buoy is still operating and initial results will be discussed here.

The 3 hour averages of salinity, as measured with the buoy to date, are shown in Figure 7.

shown. The hydrocast samples were taken at 10 m, 20 m, and 30 m, so values from 10 m and 20 m are interpolated for comparison with the 15 m sensor. Temperature sensor 3 has displayed a large upward drift from the beginning of the experiment, while the other two temperatures have remained only slightly above the freezing point for the salinities indicated. Therefore, it is felt that temperature sensor 3 is malfunctioning, so data from temperature sensor 2 has been used in calculating salinities S_2 and S_3.

The figure indicates the top 30 m is well mixed and the salinities show a gradual increase from about 32.45 o/oo to 32.73 o/oo between day 57 and day 135. The buoy measurements, especially at 30 m, agree well with the hydrocast data. On day 61, the value of S_1 interpolated from 3 hour averages is 0.044 o/oo lower than the bottle salinity, while S_2 and S_3 are 0.014 o/oo low and 0.025 o/oo low respectively. On day 89, S_1 is 0.041 o/oo low, while S_2 is 0.004 o/oo high, and S_3 is 0.007 o/oo low. On day 119, S_1 is 0.023 o/oo low, S_2 is 0.004 o/oo high, and S_3 is 0.008 o/oo low. The difference between S_1 and S_2, both measured at 30 m, is about 0.01 o/oo throughout the experiment.

For all the sensors, the mean difference between the bottle sample salinities and buoy salinities ($S_{Bottle} - S_{Buoy}$) is 0.017 o/oo and the standard deviation of the differences is 0.018 o/oo. The largest differences are associated with the data at 15 m. If only sensors 2 and 3 are considered, the differences have a mean of 0.008 o/oo and a standard deviation of 0.011 o/oo. These differences are lower than those obtained by comparing the buoy data and bottle data at Fram III. They are about the same as those found by comparing the buoy data

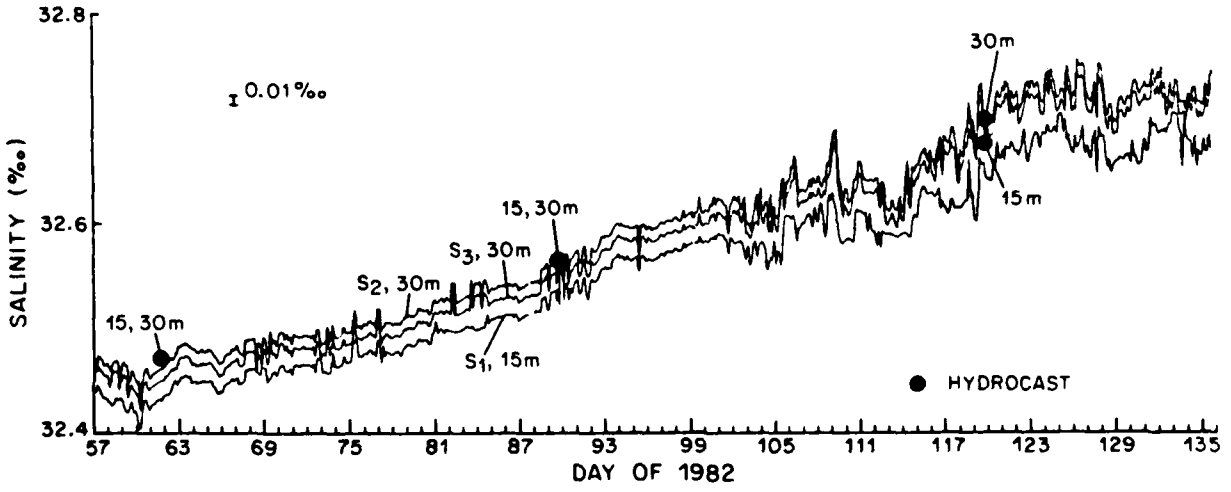

Figure 7. SALARGO3 buoy salinities at Pond Inlet, Northwest Territories plotted versus day of 1982. Salinities measured with hydrocasts at the buoy site are also shown, and agree with the buoy data.

Salinities from three hydrocasts, made by the staff of the Pond Inlet Research Establishment on days 61, 89, and 119 at the buoy site, are also

with the APS data at Fram III and are on the order of the resolution of salinity. The measurements show decreasing differences with time over the two month

period analyzed so far. This suggests that fouling has not been a problem but that, perhaps, ice accreted to the sensors at the beginning of the experiment has been a problem, particulary for the 15 m sensor.

The main difference between the hydrocasts made at Pond Inlet and those made at Fram III may be that, while the Pond Inlet water samples were analyzed soon after the casts were made, samples from Fram III were stored in polypropylene bottles for periods of up to two months before analysis. This has been found not to be a problem with some plastic bottles (Irish, personal communication) but conceivably water can evaporate through such bottles, raising the sample salinity with time. This would account for the increased offsets for the samples taken earliest at Fram III.

4. Conclusions

The Pond Inlet tests have not been concluded but so far the results of that test and the comparisons with the APS at Fram III are very promising. They suggest that the SALARGOS buoy is capable of making salinity measurements with accuracies of about 0.02 o/oo for periods of at lesst two months in the Arctic during spring conditions. Biological fouling does not appear to be a problem for these conditions. Both at Fram III and at Pond Inlet, the buoy data clearly resolves natural changes in salinity structure which have magnitudes more than ten times larger than the instrument accuracy. Currently, the temperature resolution, not fouling or other drift problems, appears to be limiting the resolution of salinity determined from temperature and conductivity measurements. Consequently the temperature resolution of the buoys will be increased by a factor of at least four for all future work. This should improve the potential accuracy of the buoy significantly.

The cause of the low salinity readings, relative to the hydrocast data at Fram III and the hydrocast data from 15 m at Pond Inlet, are still unexplained. The good agreeement of the buoy data with the Pond Inlet hydrocast data at 30m, and the fact that the calibration for conductivity sensor 2 was virtually the same for Pond Inlet as for Fram III, imply the offsets are not due to an error in sensor calibration. However, it is possible that some special application problem, such as ice adhering to the sensors, causes the low salinity readings. Errors in the hydrocast salinities, due to the type of sample bottles used, remains an important, potential cause of the offsets.

Further tests and calibrations of the instruments must be conducted in order to determine if the offsets are due to the presence of ice in the sensors or some characteristic of the sensor. The plastic sample bottles of the type used in the Fram III hydrocasts must also be tested for their ability to stop loss of water through evaporation.

Acknowledgments

The authors wish to thank Jon French for developing and running the data analysis programs used in this study. They also thank Tom Manley for providing the salinity data from Lamont-Doherty Geological Observatory. They thank Art Pederson for his advice on the use of the Seabird sensors, Clayton Paulson for his suggestions and efforts at the inception of this project and George Hobson of the Canadian Polar Continental Shelf Project for his assistance. This work was funded by the Office of Naval Research Contracts N00014-79-C-0024 and N00014-78-C-0135.

References

Irish, J. D., 1977. Moored temperature and conductivity measurements. Exposure, 5(4), 1-6.

Irish, J. D., 1981. Water column pressure measurements: CODE. EOS, 62(45), 911. (Abstract of a talk given at the 1981 AGU Fall Meeting, San Francisco, California.)

Lewis, E. L., 1980. The practical salinity scale 1978 and its antecedents. IEEE Journal of Oceanic Engineering, OE-S(1), 3-8.

Pederson, A. M. and M. C. Gregg, 1979. Development of a small in-situ conductivity instrument. IEEE Journal on Oceanic Engineering, OE-4(3), 69-75.

END

FILMED

6-85

DTIC